Review

Photoresponsive TiO_2/Graphene Hybrid Electrodes for Dual-Function Supercapacitors with Integrated Environmental Sensing Capabilities

María C. Cotto , José Ducongé , Francisco Díaz , Iro García , Carlos Neira , Carmen Morant , Francisco Márquez *

Posted Date: 4 November 2025

doi: 10.20944/preprints202511.0205.v1

Keywords: photoresponsive supercapacitors; TiO_2/graphene nanohybrids; multifunctional energy devices; VOC sensing; environmental monitoring; light-enhanced capacitance; smart wearable systems

 doi:10.20944/preprints202511.0205.v1

Review

Photoresponsive TiO_2/Graphene Hybrid Electrodes for Dual-Function Supercapacitors with Integrated Environmental Sensing Capabilities

María C. Cotto [1], José Ducongé [1], Francisco Díaz [1], Iro García [1], Carlos Neira [1], Carmen Morant [2] and Francisco Márquez [1,*]

[1] Nanomaterials Research Group, Department of Natural Sciences and Technology, Division of Natural Sciences, Technology and Environment, Universidad Ana G. Méndez-Gurabo Campus, 00778PR, USA

[2] Department of Applied Physics, Autonomous University of Madrid, and Instituto de Ciencia de Materiales Nicolás Cabrera, 28049, Spain

* Correspondence: fmarquez@uagm.edu; Tel.: +1-787-743-7979 (ext. 4250)

Abstract

The integration of energy storage and environmental sensing functions into a single device represents a critical step toward the development of autonomous smart systems. In this work, we report the design and fabrication of photoresponsive supercapacitors based on TiO_2/graphene hybrid electrodes that simultaneously deliver enhanced energy storage performance and environmental monitoring capabilities. The nanocomposite electrodes are prepared via a scalable sol-gel and hydrothermal route, followed by mild thermal treatment to optimize interface interactions and photoactivity. Under UV and visible light illumination, the devices exhibit a significant increase in specific capacitance, up to 35% enhancement, due to improved charge separation and interfacial polarization effects. Moreover, the same hybrid materials demonstrate sensitivity to volatile organic compounds (VOCs) and humidity, enabling their use as dual-function components in next-generation smart electronics. The synergistic combination of light-driven capacitive enhancement and real-time environmental response highlights the potential of these hybrid systems for self-powered, multifunctional platforms in wearable and distributed sensor networks.

Keywords: photoresponsive supercapacitors; TiO_2/graphene nanohybrids; multifunctional energy devices; VOC sensing; environmental monitoring; light-enhanced capacitance; smart wearable systems

1. Introduction

The development of advanced energy storage systems has become one of the most urgent priorities in materials science and applied chemistry, driven by the accelerating global transition towards sustainable energy and the pervasive growth of portable and autonomous electronic devices. The rising complexity of modern technologies—ranging from medical implants and wearable sensors to distributed Internet of Things (IoT) networks—requires energy storage platforms that combine high performance, long-term reliability, and multifunctionality in compact and lightweight formats [1]. Conventional electrochemical systems, particularly lithium-ion batteries, have dominated the energy storage landscape due to their relatively high energy density (100–250 Wh kg^{-1}). However, their limited power density, long charging times, and safety issues associated with flammable electrolytes motivate the exploration of complementary or alternative devices [2]. Supercapacitors, also known as electrochemical capacitors, bridge the gap between batteries and traditional capacitors by delivering high power density, rapid charging/discharging, and excellent cycling stability [3]. Two major categories exist: electric double-layer capacitors (EDLCs), where charge is stored electrostatically at the electrode/electrolyte interface, and pseudocapacitors, which involve fast and

 doi:10.20944/preprints202511.0205.v1

reversible surface redox processes [4]. Despite their outstanding power performance, conventional supercapacitors typically achieve energy densities in the range of 3–10 Wh kg^{-1}, well below that of batteries [5]. This intrinsic limitation restricts their applicability in autonomous devices that require prolonged operation without frequent recharging.

Addressing this challenge requires not only improvements in electrode materials but also the redefinition of device functionality. Recent years have witnessed the emergence of photoresponsive supercapacitors, which exploit the interaction between light and electrochemical processes to enhance energy storage capacity or even provide self-charging capability. By integrating photoactive materials into electrode architectures, such devices can generate additional charge carriers under illumination, leading to improved capacitance and energy output [5]. Mechanisms such as photogenerated electron–hole pair separation, interfacial polarization, and photodoping have been proposed to explain the enhancement of capacitance under light irradiation [6].

Among the photoactive materials explored, titanium dioxide (TiO_2) has been extensively investigated due to its stability, abundance, non-toxicity, and well-understood photocatalytic properties [7]. TiO_2 exhibits three main crystalline forms—anatase, rutile, and brookite—each with distinct surface energies, band structures, and catalytic activities. Anatase, with a bandgap of ~3.2 eV, is the most widely studied due to its superior photocatalytic activity under ultraviolet (UV) light, while rutile (~3.0 eV) demonstrates higher thermodynamic stability [8]. However, pristine TiO_2 suffers from significant drawbacks, such as low electronic conductivity and rapid recombination of photogenerated electron–hole pairs, which reduce its efficiency in electrochemical and photocatalytic processes [9].

To overcome these limitations, researchers have turned to hybrid materials combining TiO_2 with highly conductive carbon-based nanostructures, especially graphene and its derivatives. Graphene, a two-dimensional sheet of sp^2-bonded carbon atoms, provides exceptional conductivity (~10^6 S m^{-1}), ultrahigh surface area (~2600 m^2 g^{-1}), and remarkable mechanical properties [10]. Its incorporation into TiO_2-based electrodes enhances charge transport, suppresses electron–hole recombination, and improves the structural integrity of the composite under repeated cycling [11]. Moreover, defect sites and functional groups in reduced graphene oxide (rGO) facilitate strong interfacial coupling with TiO_2, leading to synergistic improvements in both electrochemical and photoelectrochemical performance [12].

The coupling of TiO_2 and graphene not only enhances energy storage characteristics but also paves the way for dual-functionality. Recent work has demonstrated that such hybrids can operate as both energy storage devices and environmental sensors. TiO_2 nanostructures exhibit intrinsic sensitivity to humidity, oxygen, and volatile organic compounds (VOCs), while graphene provides high surface-to-volume ratio and tunable surface chemistry, making the hybrid suitable for capacitive sensing applications [13] Graphene-based wireless bacteria detection on tooth enamel. In these systems, adsorption of analytes leads to detectable variations in capacitance, effectively integrating energy storage and environmental monitoring into a single device [14].

From a broader perspective, multifunctional supercapacitors based on TiO_2/graphene hybrids align with the global push towards self-powered and intelligent electronics. The ability to harvest energy from ambient light, store it, and simultaneously monitor environmental conditions represents a paradigm shift in the design of autonomous systems. These devices hold promise for applications ranging from wearable health monitoring to distributed environmental sensing in smart cities, and even aerospace platforms where weight, multifunctionality, and reliability are critical [15].

Given this context, the present review aims to provide a comprehensive assessment of photoresponsive TiO_2/graphene hybrid electrodes. Specifically, it discusses their working principles, material properties, fabrication strategies, dual-function capabilities, and performance benchmarks. Special attention is devoted to the underlying mechanisms of photo-induced capacitance enhancement and the integration of sensing functions with storage. By consolidating current knowledge, identifying challenges, and outlining future directions, this review seeks to contribute to the rational design of multifunctional, next-generation energy devices.

 doi:10.20944/preprints202511.0205.v1

2. Fundamentals of Photoresponsive Supercapacitors

2.1. Working Principles of Supercapacitors – EDLCs vs Pseudocapacitors

The operation of supercapacitors relies on two distinct but often complementary charge storage mechanisms: the formation of an electrochemical double layer and the occurrence of fast, reversible faradaic processes. Devices dominated by the first mechanism are known as electrical double-layer capacitors (EDLCs), while those exploiting the second are referred to as pseudocapacitors. Understanding the interplay between these two modes of energy storage is essential to rationalize the performance of emerging photoresponsive hybrid systems such as TiO_2/graphene-based supercapacitors. In EDLCs, the capacitance originates from electrostatic charge accumulation at the electrode–electrolyte interface. When a potential is applied, ions in the electrolyte arrange themselves near the charged surface of the electrode, creating what is known as the Helmholtz double layer. The effective separation distance is only a few angstroms, which allows very high capacitance per unit area. The classical expression $C=\varepsilon A/d$ illustrates that maximizing the accessible surface area A and minimizing the separation distance d are key to achieving high capacitance. This is why carbon-based materials, especially graphene, are the cornerstone of EDLC technology: they provide extremely large surface areas, excellent conductivity, and chemical stability, enabling specific capacitances of several hundred farads per gram under optimized conditions [1]. The purely electrostatic nature of this storage process grants EDLCs outstanding cycle life, often exceeding 10^5 cycles with minimal degradation, and ultra-fast charge/discharge rates. However, their energy density is relatively modest, typically 5–10 Wh kg^{-1}, which limits their application in scenarios demanding sustained energy delivery [16]. In contrast, pseudocapacitors exploit fast faradaic reactions occurring either on the electrode surface or within near-surface layers. These include redox reactions, ion electrosorption with charge transfer, and shallow intercalation processes. Unlike batteries, pseudocapacitors do not involve phase transformations or irreversible chemical changes; the faradaic processes are highly reversible and kinetically fast. The result is a much higher capacitance than EDLCs can provide, often one to two orders of magnitude greater per surface area unit. Classical examples include transition metal oxides such as RuO_2, MnO_2, and TiO_2, as well as conducting polymers like polyaniline or polypyrrole [17]. The main advantage of pseudocapacitance lies in its ability to dramatically enhance energy density, often bridging the gap between batteries and EDLCs. However, this comes at the expense of durability: faradaic processes typically induce gradual degradation of the electrode structure or chemical composition, leading to shorter cycle lifetimes compared with EDLC-based devices [18]. In practice, many high-performance devices combine both mechanisms. Hybrid supercapacitors intentionally integrate EDLC-active materials, such as graphene or activated carbons, with pseudocapacitive components, such as TiO_2 or MnO_2, to exploit the high power of EDLCs and the enhanced energy of pseudocapacitors. The synergy between these two contributions often results in improved performance metrics that cannot be achieved by either mechanism alone [19]. The hybridization strategy is particularly relevant in the development of multifunctional and photoresponsive systems. In the case of TiO_2/graphene electrodes, graphene ensures fast electron transport and extensive electrostatic charge storage, while TiO_2 contributes additional pseudocapacitance through reversible surface redox processes. Moreover, TiO_2 is photoactive: upon illumination with UV or visible light, photogenerated electron–hole pairs further enhance charge separation and reduce recombination, leading to a measurable increase in capacitance. This light-induced modulation of capacitance not only boosts energy storage performance but also opens the possibility of integrating environmental sensing functions, as TiO_2 surfaces are known to interact with volatile organic compounds and humidity [20]. The distinction between EDLCs and pseudocapacitors, therefore, is not merely of academic interest but provides the conceptual framework to design multifunctional devices. By carefully tailoring the contributions of electrostatic and faradaic processes, and by incorporating photoresponsive materials, next-generation supercapacitors can simultaneously achieve high power, enhanced energy density, responsiveness to environmental stimuli, and durability suitable for wearable and distributed sensing platforms. A

 doi:10.20944/preprints202511.0205.v1

concise comparison of the key features of EDLCs, pseudocapacitors, and hybrid/photoresponsive devices is provided in Table S1, which highlights their respective charge storage mechanisms, materials, performance metrics, cycle life, and additional functionalities. The table emphasizes that while EDLCs and pseudocapacitors each offer distinct advantages and limitations, hybrid systems—particularly photoresponsive TiO_2/graphene composites—represent a versatile and promising pathway toward multifunctional energy storage devices with integrated sensing capabilities.

2.2. Mechanisms of Photo-Induced Capacitance Enhancement

The enhancement of capacitance under light irradiation in photoresponsive supercapacitors arises from the unique interaction between semiconductor photoactivity and electrochemical charge storage processes. When hybrid materials such as TiO_2/graphene are exposed to illumination, a series of electronic and interfacial phenomena are triggered that profoundly modify the dynamics of charge storage. At the heart of this effect is the generation of photocarriers in the semiconductor, which under appropriate conditions can be separated and transferred to conductive supports such as graphene. Photons with energies equal to or higher than the TiO_2 band gap (~3.2 eV for anatase) excite electrons from the valence band to the conduction band, leaving behind positively charged holes. The resulting electron–hole pairs, if not recombined, substantially increase the density of free carriers available to participate in electrochemical processes at the electrode–electrolyte interface. Graphene, owing to its high conductivity and delocalized π-electron system, acts as an effective sink and transport channel for photogenerated electrons, thereby reducing recombination losses and extending carrier lifetimes. This cooperative interaction ensures that a significant fraction of the photoexcited electrons contribute to electrochemical double-layer formation and pseudocapacitive reactions, leading to measurable increases in capacitance, often reported in the range of 20–40% under UV or visible illumination [21].

In addition to the generation of carriers, illumination also reshapes the interfacial polarization phenomena that govern energy storage in supercapacitors. In classical EDLCs, the capacitance is limited by the electrostatic alignment of electrolyte ions at the electrode surface. The introduction of photogenerated carriers in TiO_2 alters local electric fields, reinforcing the polarization at the semiconductor–electrolyte boundary. This "photoinduced polarization" manifests as a strengthening of the double layer, effectively increasing the apparent capacitance. Nanostructured TiO_2 architectures, such as nanotubes, nanowires, or mesoporous films, are particularly effective in amplifying this effect due to their high density of active surface sites. Moreover, the photogenerated holes at the TiO_2 surface can interact with adsorbed molecules such as water, hydroxyls, or even volatile organic compounds, modifying surface dipoles and leading to dynamic shifts in interfacial polarization. When coupled with graphene, these polarization effects are spread across a highly conductive carbon network, ensuring that the photoinduced charges are efficiently distributed and that polarization occurs over a larger effective interfacial area [22]. This dynamic interplay between ionic adsorption and electronic carrier redistribution is one of the main reasons why hybrid electrodes show stronger light-enhanced capacitance compared to bare semiconductors.

A further, and in many ways more subtle, mechanism is photodoping, which arises when photogenerated electrons or holes become trapped in defect states, oxygen vacancies, or interfacial sites within the semiconductor. In the case of TiO_2, electrons trapped in oxygen vacancies shift the Fermi level closer to the conduction band, effectively increasing electronic conductivity and lowering the charge-transfer resistance at the electrode/electrolyte interface. This phenomenon, often described as "photoinduced doping," can persist beyond the illumination period, leading to long-lived conductive states and a memory effect in capacitance, where enhanced charge storage is maintained for some time even after the light is switched off [23,24]. Such persistent photoconductivity is particularly relevant for multifunctional applications, as it enables hybrid electrodes not only to store energy more efficiently under light but also to retain enhanced responsiveness in the dark. In addition, photodoping dynamically modifies the band alignment between TiO_2 and graphene, facilitating more favorable electron injection and faster interfacial kinetics. These shifts reduce

 doi:10.20944/preprints202511.0205.v1

internal resistance and improve the overall efficiency of both electrostatic and faradaic processes. The combined effect of these mechanisms creates a highly synergistic scenario. Photogenerated carriers increase the available charge density; surface polarization strengthens the double layer and enhances ion–electron coupling at the interface; and photodoping stabilizes charges, lowers resistance, and extends the lifetime of photoinduced states. Rather than being isolated, these processes reinforce one another: graphene extracts and delocalizes photogenerated electrons, preventing recombination and spreading polarization; TiO_2 provides a dense network of active sites where interfacial fields and photodoping can occur; and the hybrid architecture allows these microscopic effects to translate into macroscopic capacitance enhancement. Under continuous illumination, the capacitance of TiO_2/graphene devices has been shown to increase by as much as 35%, while maintaining stability over thousands of cycles [18,19]. Perhaps most significantly, these same photo-induced processes also confer additional functionalities beyond energy storage. The interaction of photogenerated holes with adsorbed species makes TiO_2-based electrodes inherently sensitive to environmental factors such as humidity and volatile organic compounds. Changes in adsorption alter polarization and photodoping dynamics, which can be transduced into measurable shifts in capacitance. As a result, TiO_2/graphene photoresponsive supercapacitors operate simultaneously as energy storage devices and environmental sensors. Recent work by Al-Hamry et al. [20] demonstrated that TiO_2/graphene oxide nanocomposites act as highly sensitive humidity sensors, confirming that environmental monitoring can be embedded directly into energy storage platforms without additional components. This multifunctionality is particularly relevant for next-generation wearable and distributed electronics, where self-powered, adaptive, and environmentally aware devices are in increasing demand.

Taken together, the mechanisms of charge separation, interfacial polarization, and photodoping illustrate the fundamental basis of light-enhanced supercapacitor performance. They show how careful integration of photoactive oxides with conductive carbons like graphene can transform supercapacitors from passive energy storage devices into active, multifunctional systems. By exploiting photon–matter interactions at the nanoscale, it becomes possible to design electrodes that not only store more energy under illumination but also sense and respond to their environment, paving the way for self-sufficient smart technologies.

2.3. Influence of UV vs. Visible Light

The spectral region of incident light strongly determines the mechanisms and magnitude of photo-induced capacitance in supercapacitors. Ultraviolet (UV) photons, with wavelengths below 400 nm, have sufficient energy to directly excite wide-bandgap semiconductors such as TiO_2 and ZnO (bandgap ~3.0–3.2 eV), leading to efficient electron–hole pair generation and strong capacitance enhancement. In contrast, visible light comprises about 45% of the solar spectrum but has lower photon energy, which makes it far more abundant and sustainable yet requires careful material engineering to harvest effectively. Under UV light, wide-bandgap semiconductors undergo direct band-to-band transitions in which photogenerated carriers are efficiently separated and accumulated in the electrode or at the electrode–electrolyte interface. A clear demonstration of this effect was reported in ZnO-based photo-supercapacitors, where the specific capacitance of ZnO nanofibers increased by approximately 2.4 times and that of ZnO nanowires nearly doubled under UV irradiation. Charge–discharge times decreased by almost fivefold, while the coulombic efficiency improved from about 33% to over 100%, underscoring the strong role of UV photons in promoting charge storage processes [25]. These improvements were attributed to enhanced photocarrier generation, reduced charge transfer resistance, and extended diffusion pathways observed in impedance spectra. Despite these advantages, UV light constitutes less than 5% of natural sunlight, which limits the sustainability of UV-driven systems. This makes the development of visible-light responsive photo-supercapacitors an essential step toward practical devices. Several strategies have been explored, including bandgap engineering through doping with transition metals such as Fe, Co, or V, or non-metals such as N, S, and C, which introduce intermediate states that allow absorption of

 doi:10.20944/preprints202511.0205.v1

sub-bandgap photons. Another approach relies on coupling wide-bandgap oxides with narrow-bandgap semiconductors such as MoS_2, CdS, or g-C_3N_4, enabling the transfer of photogenerated carriers across heterointerfaces. Hybridization with conductive carbonaceous nanostructures such as graphene, reduced graphene oxide, and carbon nanotubes has also proven effective, as these materials extend the optical absorption range while providing rapid charge transport pathways. The potential of visible-light activation has been convincingly demonstrated in recent studies. A hybrid photocapacitor integrating a dye-sensitized solar cell with an asymmetric supercapacitor achieved a charging voltage of 920 mV under indoor light illumination (1000 lux) and a power conversion efficiency exceeding 30%, allowing continuous operation of a microcontroller without external batteries [26]. Another example involves the use of germanane and its derivatives as photoactive electrodes in hybrid zinc-ion capacitors. When irradiated with visible light at 435 nm, capacitance increased by up to 52%, retention of 91% was maintained after 3000 cycles, and maximum capacitance values reached nearly 6000 mF g^{-1}, with charging voltages approaching 1 V [27]. In addition, heterojunctions combining polymeric carbon nitride with MXene nanosheets have been shown to drive efficient photo-charging under visible light via interfacial charge transfer, leading to highly efficient photo-rechargeable supercapacitors [28].

Taken together, these results illustrate a fundamental tradeoff. UV irradiation provides straightforward, highly efficient carrier generation but is scarce under solar illumination, while visible light is abundant but requires advanced materials engineering to exploit. Progress in heterojunction design, doping, hybrid nanostructures, and 2D semiconductors demonstrates that visible-light harvesting can enable sustainable, solar-compatible, and multifunctional photo-supercapacitors. Transitioning from UV-driven to visible-light-responsive devices is therefore not only an optimization of efficiency but also a paradigm shift toward real-world applications in energy storage, sensing, and autonomous electronics.

2.4. Distinction from Photo-Rechargeable Batteries

Photo-active supercapacitors must be clearly distinguished from photo-rechargeable batteries, even though both concepts rely on coupling light harvesting with energy storage. The key difference lies in the underlying charge storage mechanism. Supercapacitors store energy electrostatically at the electrode–electrolyte interface in electric double layers or through fast surface redox reactions, enabling rapid charging and discharging and high cyclability. In contrast, photo-rechargeable batteries operate through bulk redox processes within electrode materials, where photogenerated carriers directly drive insertion or extraction of ions such as Li^+, Na^+, or Zn^{2+}, resulting in higher energy density but typically slower kinetics. In photo-active supercapacitors, light irradiation enhances the capacitance by increasing carrier density, promoting interfacial polarization, or driving charge transfer across engineered heterojunctions. This effect is transient and strongly dependent on the illumination conditions; once the light source is removed, the additional capacitance gain decays. In photo-rechargeable batteries, however, photons directly participate in driving faradaic reactions, enabling the storage of solar energy in the form of chemical energy. A well-studied case is the use of TiO_2 photoanodes in lithium-ion systems, where photogenerated electrons facilitate Li^+ insertion into TiO_2, leading to direct photocharging of the battery [29]. The differences in performance metrics further highlight this distinction. Performance metrics also highlight the fundamental distinction. Photo-rechargeable batteries typically achieve higher energy densities, often exceeding 150 Wh kg^{-1}, but are limited in power density and cycle life. Photo-supercapacitors, in contrast, deliver power densities in the kW kg^{-1} range and demonstrate cycling stability beyond 10^5 cycles, although their energy densities remain comparatively lower. An illustrative example of integrated photo-energy storage is the work of Plebankiewicz et al., who combined silicon solar cells with supercapacitors in a photo-rechargeable architecture, demonstrating the potential of hybrid systems [30]. Another fundamental difference is architectural. Photo-rechargeable batteries often employ semiconductor photoelectrodes directly interfaced with redox-active insertion compounds, requiring careful band alignment to enable ion intercalation. In photo-active supercapacitors, the illumination is used to

 doi:10.20944/preprints202511.0205.v1

generate excess carriers in the electrode material or its surface states, which then contribute to enhanced double-layer formation or pseudocapacitance. This difference also influences application scenarios. While photo-rechargeable batteries are aimed at long-term solar energy storage, such as off-grid power supply, photo-active supercapacitors are better suited for short-term, high-power applications, including self-powered sensors, transient electronics, and hybrid systems integrated with photovoltaics.

This conceptual distinction is important for guiding future research. Photo-rechargeable batteries will continue to evolve toward higher efficiencies through material design, but challenges such as slow kinetics, complex architectures, and stability under prolonged illumination remain. Photo-active supercapacitors, while offering lower energy density, provide unique opportunities for real-time energy buffering and multifunctional integration, where fast response and robustness outweigh the need for long-duration storage. The complementary development of both technologies will therefore be essential for building integrated solar-powered energy storage systems that combine the high-power performance of supercapacitors with the high energy density of batteries.

3. TiO_2-Based Photoactive Materials

3.1. Structural, Optical, and Electrochemical Properties of TiO_2 (Anatase, Rutile, Brookite)

Titanium dioxide (TiO_2) is a prototypical photoactive material that crystallizes in three main polymorphs—anatase, rutile, and brookite—each displaying distinct structural, optical, and electrochemical features that strongly influence their performance in photo-assisted energy storage systems. All three structures are composed of TiO_6 octahedra but differ in their connectivity and distortion, which in turn modulate surface energy, defect chemistry, and electronic band structure. Anatase has a tetragonal structure characterized by corner- and edge-sharing TiO_6 octahedra with slight distortions, resulting in a relatively open framework that facilitates high surface area and enhanced reactivity. Rutile, also tetragonal, adopts a more compact arrangement with linear Ti–O–Ti bonds, making it the thermodynamically most stable polymorph at elevated temperatures. Brookite, in contrast, exhibits an orthorhombic structure with a more complex network of distorted TiO_6 units, giving rise to intrinsic lattice strain and a high density of surface-active sites. These differences in atomic arrangement lead to variations in particle morphology, defect distribution, and reactivity under illumination [7]. From an optical standpoint, TiO_2 is a wide-bandgap semiconductor, with anatase showing a bandgap of ~3.2 eV, rutile ~3.0 eV, and brookite ~3.1 eV. These values restrict absorption mainly to the ultraviolet region of the solar spectrum (<5%), limiting practical solar-driven applications. Nevertheless, anatase is generally considered the most photoactive polymorph because its conduction band minimum lies at a higher energy than rutile, leading to stronger reducing power and more efficient charge separation. Rutile, while less efficient in photogeneration, benefits from a slightly narrower bandgap that extends absorption into longer UV wavelengths. Brookite, although less studied, has attracted growing interest due to its intrinsic lattice distortion, which enhances electron–hole separation and enables synergistic effects when combined with other polymorphs. Indeed, mixed-phase systems such as anatase–rutile or anatase–brookite heterojunctions often outperform single-phase materials by promoting internal electric fields that suppress recombination [31]. Electrochemically, the three polymorphs also display distinct behaviors. Anatase is well known for its capability to accommodate small cations (Li^+, Na^+, H^+) through reversible intercalation, which underpins its use in both batteries and pseudocapacitive electrodes. Its relatively open structure and high surface area enable fast ion transport and high cycling stability. Rutile, owing to its dense atomic packing, is less favorable for ion insertion but exhibits excellent chemical stability in aqueous environments, making it attractive for long-term durability in supercapacitors and hybrid photoelectrochemical systems. Brookite combines features of both, with higher surface energy and defect density that provide abundant adsorption sites for ions, potentially enhancing pseudocapacitance and light-assisted charge storage. The electrochemical response of TiO_2 electrodes is further enhanced at the nanoscale, where morphologies such as nanotubes, nanorods, and

 doi:10.20944/preprints202511.0205.v1

mesoporous films improve ion accessibility and charge separation, while defect engineering (oxygen vacancies, Ti^{3+} states) enhances conductivity and facilitates photocarrier transport [21]. Overall, anatase is the most exploited phase for photo-assisted supercapacitor applications due to its superior electronic properties, but recent studies highlight the advantages of mixed-phase and defect-engineered systems that combine the strengths of anatase, rutile, and brookite. These polymorphs, through their structural, optical, and electrochemical complementarities, continue to provide a versatile platform for advancing TiO_2-based photoactive materials in energy storage applications.

3.2. Role of Crystallinity, Particle Size, and Surface Area

The performance of TiO_2-based photoactive materials in energy storage devices is not only governed by their intrinsic band structure but is also highly sensitive to microstructural parameters such as crystallinity, particle size, and surface area. These factors determine the density of active sites, the transport pathways for electrons and ions, and the overall balance between charge storage capacity, rate capability, and cycling stability.

Crystallinity plays a decisive role in charge carrier dynamics. Highly crystalline TiO_2 typically exhibits fewer structural defects, which reduces charge carrier recombination and promotes efficient electron transport. For example, Chen and Mao highlighted that improved crystallinity enhances the electron diffusion length, thereby facilitating efficient charge separation and transfer in anatase nanoparticles [21]. However, excessive crystallinity can also reduce the density of surface hydroxyl groups and active defect sites (such as Ti^{3+} centers or oxygen vacancies), which are crucial for pseudocapacitive charge storage and surface redox reactions. Thus, an optimal trade-off between crystallinity and defect density is required to maximize both conductivity and capacitance.

Particle size is equally important. Reducing the crystallite size to the nanoscale increases the specific surface area and shortens the diffusion distance for charge carriers and ions, resulting in improved electrochemical kinetics. Nanoparticles and nanocrystals with diameters below 20 nm exhibit quantum confinement effects, which shift the bandgap to higher energies, enhancing photocatalytic activity under UV light but limiting visible-light absorption. Conversely, larger crystallites reduce surface area but may favor bulk ion insertion processes due to reduced recombination at grain boundaries. Studies on TiO_2 nanocrystals have shown that optimal sizes around 10–20 nm balance high surface reactivity with efficient charge transport, leading to enhanced performance in hybrid energy storage applications [32].

Surface area and porosity are central to the capacitive behavior of TiO_2 electrodes. A larger accessible surface increases the number of electrochemically active sites for double-layer formation and surface faradaic reactions, while mesoporous architectures improve electrolyte infiltration and ion diffusion. The introduction of hierarchical porosity—micropores for ion adsorption, mesopores for ion transport, and macropores for electrolyte diffusion—has been shown to markedly enhance capacitance and cycling stability. For instance, Wu et al. demonstrated that mesoporous TiO_2–carbon composites provide high surface area and improved electron pathways, enabling significant enhancement in both energy and power densities [33]. The interplay between these three factors becomes particularly evident when evaluating different TiO_2 morphologies. Nanotubes, nanowires, and mesoporous films often exhibit higher specific surface area and directional electron transport compared to bulk particles, effectively reducing diffusion limitations and enhancing charge separation. However, excessive downsizing can cause structural instability, particle aggregation, and reduced electrical connectivity. Therefore, optimal performance in photoactive supercapacitors is achieved through the rational engineering of crystallinity, particle dimensions, and porous architectures, often complemented by defect engineering and surface functionalization to fine-tune charge transfer dynamics [34,35].

In conclusion, crystallinity, particle size, and surface area are intimately connected parameters that control the optical absorption, charge carrier dynamics, and electrochemical response of TiO_2. Optimizing these properties not only enhances UV-light-driven capacitance but also provides a

 doi:10.20944/preprints202511.0205.v1

platform for coupling with sensitizers and carbon-based materials to extend activity into the visible range, thereby broadening the application potential of TiO_2-based photoactive supercapacitors.

3.3. Bandgap Tuning via Doping (e.g., N, F, Metals)

One of the main limitations of pristine TiO_2 is its wide bandgap (~3.0 eV for rutile and ~3.2 eV for anatase), which restricts its optical absorption mainly to the ultraviolet region, accounting for less than 5% of the solar spectrum. To extend its activity into the visible-light range and improve its suitability for photoactive energy storage, bandgap tuning through doping has been extensively investigated. Doping introduces impurity levels within the electronic structure of TiO_2, modifying the positions of the conduction and valence bands, altering charge carrier dynamics, and facilitating absorption of sub-bandgap photons. Non-metal doping has received particular attention for visible-light activation. Nitrogen doping is among the most widely studied strategies; substitutional N atoms introduce localized states above the valence band maximum of TiO_2, effectively narrowing the bandgap and shifting absorption into the visible range. Asahi et al. were the first to demonstrate that N-doped TiO_2 exhibits visible-light photocatalytic activity, attributing this effect to the mixing of N 2p states with O 2p orbitals [36]. Other non-metals, such as fluorine, carbon, and sulfur, have also been employed. Fluorine, in particular, enhances the surface acidity and modifies surface states, improving charge separation and electrochemical reactivity without drastically altering the bandgap [37]. Metal doping offers another effective pathway. Transition metals such as Fe, Cr, V, and Mn can introduce discrete donor or acceptor states within the bandgap, thereby extending light absorption into the visible region. However, the incorporation of transition metal dopants must be carefully optimized, as excessive doping often promotes charge carrier recombination and reduces photo-efficiency. For example, Fe^{3+} ions can serve as shallow traps for electrons, enhancing charge separation, while higher doping levels lead to recombination centers that suppress activity. Choi et al. demonstrated that dopants such as V^{5+}, Cr^{3+}, and Fe^{3+} significantly alter photocatalytic responses, with the effect strongly dependent on dopant concentration [37]. Noble metals such as Au, Ag, and Pt, though not classical dopants, have also been employed to create localized surface plasmon resonance (LSPR) effects, enabling visible and near-infrared activation by hot electron injection into TiO_2 conduction bands. Co-doping strategies have been developed to overcome the limitations of single-element doping, such as localized recombination. By introducing two complementary dopants—such as N with transition metals or F with cations—it is possible to simultaneously narrow the bandgap and stabilize charge carriers, leading to more efficient utilization of visible light. Khan et al. reviewed how non-metal/metal co-doping provides synergistic effects that enhance both photocatalytic and electrochemical performance [38]. For photoactive supercapacitors, bandgap-tuned TiO_2 electrodes demonstrate improved visible-light responsivity, enhanced charge accumulation, and better interfacial redox activity. By tailoring the dopant type and concentration, it is possible to maximize light harvesting while maintaining conductivity and cycling stability. Ultimately, doping strategies—whether based on anion substitution, cation incorporation, or hybrid co-doping—represent a crucial direction in designing TiO_2-based photoactive materials for next-generation energy storage devices.

3.4. Synthesis Methods: Sol-Gel, Hydrothermal, Anodization, Laser-Assisted, etc.

The synthesis route of TiO_2 has a profound impact on its crystallinity, morphology, surface area, and defect distribution, which ultimately determine its structural, optical, and electrochemical properties. Different synthetic strategies provide control over phase composition (anatase, rutile, brookite), particle size, porosity, and dopant incorporation, enabling the fine-tuning of TiO_2 for photoactive supercapacitor applications. Among the most relevant approaches are sol–gel synthesis, hydrothermal methods, anodization, and laser-assisted processes. The sol–gel method is one of the most versatile techniques for fabricating TiO_2 powders, thin films, and nanostructured coatings. It involves hydrolysis and condensation of titanium precursors, such as titanium isopropoxide or titanium butoxide, followed by controlled drying and calcination. The process allows precise control

 doi:10.20944/preprints202511.0205.v1

of stoichiometry and facilitates doping with non-metals or metals at the molecular level. Sol–gel-derived TiO_2 generally crystallizes as anatase at moderate temperatures, with high surface area and tunable porosity. However, the method is sensitive to processing conditions, and high-temperature treatments required for crystallization often reduce surface area and introduce phase transformation into rutile [39]. The hydrothermal and solvothermal methods are widely used to produce TiO_2 nanoparticles, nanorods, and hierarchical architectures under high-temperature and high-pressure aqueous conditions. These processes yield highly crystalline materials with well-defined morphologies without requiring post-annealing. Hydrothermal synthesis is particularly effective for fabricating brookite and anatase nanostructures, as well as for doping with heteroatoms and hybridizing with carbonaceous materials. Tailored morphologies such as nanorods and nanoflowers enhance surface area and directional electron transport, improving photoelectrochemical performance [40]. Anodization of titanium foils in fluoride-containing electrolytes provides a straightforward route to highly ordered TiO_2 nanotube arrays, which are directly grown on conductive substrates. These vertically aligned nanotubes offer large surface area, excellent electron transport pathways, and strong mechanical adhesion to the current collector, making them particularly suitable for supercapacitor electrodes. The geometry of the nanotubes (length, diameter, wall thickness) can be tuned by adjusting anodization voltage, electrolyte composition, and duration. Roy et al. provided a comprehensive overview of TiO_2 nanotube synthesis and applications, emphasizing their role in photoelectrochemical and energy storage devices [35]. Laser-based treatments have gained prominence as advanced methods to engineer TiO_2 surfaces, introducing defect sites that enhance visible-light response. Pulsed laser irradiation, especially using femtosecond lasers, can induce localized surface modifications without affecting the bulk material. Notably, femtosecond laser treatment of TiO_2 colloids has been shown to generate stable, dark-colored TiO_2 nanostructures (often described as "black TiO_2") through the controlled creation of oxygen vacancies and surface disorder—significantly narrowing the optical bandgap while retaining crystal phase integrity [41]. Additionally, pulsed laser ablation in liquids offers a green and versatile route to produce colloidal TiO_2 nanoparticles with pristine surfaces, free from chemical residues, which is advantageous for applications in photocatalysis and electrochemical energy storage [42]. Other advanced methods, such as flame spray pyrolysis, chemical vapor deposition (CVD), and atomic layer deposition (ALD), have also been employed to fabricate TiO_2 nanostructures with precise dimensional control and excellent scalability. Flame spray pyrolysis allows large-scale production of TiO_2 nanoparticles with controlled crystallinity and surface area, making it attractive for practical applications. CVD techniques provide conformal and uniform TiO_2 coatings on complex substrates, while ALD offers sub-nanometer thickness control, enabling the deposition of pinhole-free and highly uniform TiO_2 films. These approaches are particularly useful for producing thin coatings on electrodes, improving interfacial stability, and integrating TiO_2 into hybrid energy storage and photoelectrochemical architectures [43–45]. As a visual summary of laser-assisted routes relevant to TiO_2 processing and defect engineering, the main schemes for LAL (laser ablation in liquids), LFL (laser fragmentation in liquids), LML (laser melting in liquids), and LDL (laser defect engineering in liquids) are compiled in Figure 1.

 doi:10.20944/preprints202511.0205.v1

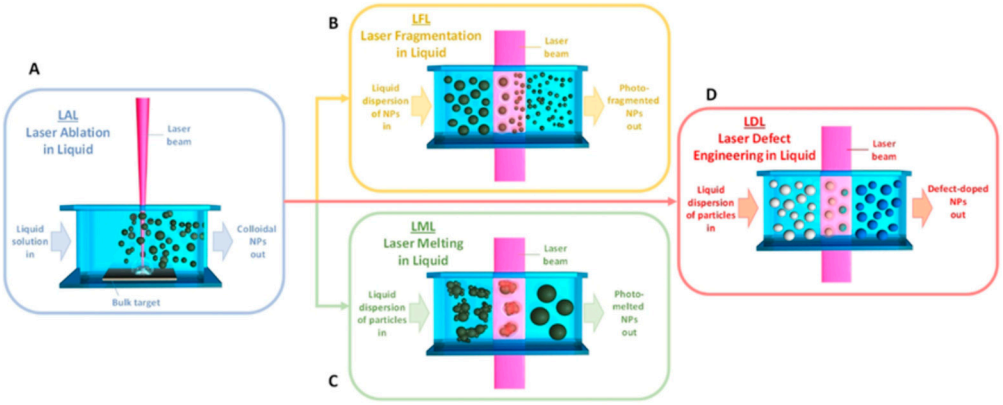

Figure 1. Schematic overview of laser-in-liquid strategies applicable to TiO_2 processing: (A) laser ablation in liquids (LAL), (B) laser fragmentation in liquids (LFL), (C) laser melting in liquids (LML), and (D) laser defect engineering in liquids (LDL). (Adapted with permission from ref. [42], Wiley 2020).

In summary, the choice of synthesis method dictates the phase composition, crystallinity, particle size, and surface properties of TiO_2. Sol–gel offers compositional flexibility, hydrothermal routes enable well-crystallized nanostructures, anodization produces ordered nanotube arrays with excellent interfacial properties, and laser-assisted processes create defect-engineered TiO_2 with extended optical response. Rational selection and combination of these methods allow the design of advanced TiO_2 electrodes with optimized light absorption, charge transport, and electrochemical performance for photoactive supercapacitor applications.

3.5. Challenges: Charge Recombination, Conductivity Limitations

Despite its wide use and advantages, TiO_2 as a photoactive material faces two critical challenges that limit its performance in photo-supercapacitors and related energy storage systems: rapid charge recombination and intrinsically low electrical conductivity. Charge recombination remains one of the most severe bottlenecks in TiO_2-based systems. Photogenerated electron–hole pairs tend to recombine within picoseconds to nanoseconds, especially in bulk materials or when surface traps act as recombination centers. This rapid recombination drastically reduces the quantum efficiency of photo-induced processes and thus lowers the contribution of light to charge storage. Even in nanostructured TiO_2, where reduced diffusion lengths improve carrier extraction, surface and grain boundary defects often promote recombination pathways. Strategies such as heterojunction engineering, coupling with carbonaceous conductors (graphene, CNTs, carbon black), and introducing oxygen vacancies have been shown to prolong carrier lifetimes and enhance interfacial charge transfer [21,31]. Electrical conductivity limitations also hinder the efficiency of TiO_2. As a wide-bandgap semiconductor, TiO_2 has very low intrinsic conductivity (~10^{-5} to 10^{-7} S cm^{-1}), which restricts electron mobility and increases internal resistance in electrochemical devices. This limitation leads to poor rate capability and reduces the achievable power density in photo-supercapacitors. Several approaches have been pursued to overcome this issue: (i) doping with transition metals (Fe, Nb, Ta) to enhance carrier concentration, (ii) hydrogenation or reduction treatments to create Ti^{3+} states and oxygen vacancies that improve n-type conductivity, and (iii) hybridization with conductive scaffolds such as reduced graphene oxide or conducting polymers. Notably, hydrogenated "black TiO_2" demonstrates orders-of-magnitude higher conductivity and improved visible-light absorption, offering a promising pathway for photoactive energy storage [32]. In addition to recombination and conductivity issues, there is also a challenge in balancing high surface area with electrical continuity. Nanostructured TiO_2 architectures—such as nanoparticles, nanotubes, or mesoporous films—provide abundant active sites and short diffusion lengths, but excessive downsizing often leads to particle aggregation, poor percolation networks, and instability under

 doi:10.20944/preprints202511.0205.v1

long-term cycling. This trade-off between surface activity and charge transport efficiency continues to be a central limitation for TiO_2 electrodes in photo-supercapacitors.

Addressing these challenges requires integrating defect engineering, heterostructure design, and hybridization with conductive frameworks. While significant progress has been made, further optimization is necessary to simultaneously achieve low recombination, high conductivity, and structural robustness in TiO_2-based photoactive materials for next-generation supercapacitors.

4. Graphene and Nanocarbon Enhancers

4.1. Role of Graphene/rGO/CNTs in Improving Conductivity and Charge Transport

One of the major limitations of pristine TiO_2 and other wide-bandgap photoactive oxides is their intrinsically low electrical conductivity, which hinders charge transport and limits their rate capability in energy storage devices. To overcome this drawback, conductive nanocarbon materials such as graphene, reduced graphene oxide (rGO), and carbon nanotubes (CNTs) have been widely integrated with TiO_2 to form hybrid architectures. These carbonaceous enhancers act as conductive backbones that facilitate electron mobility, suppress charge recombination, and improve overall device performance. Graphene is a two-dimensional sheet of sp^2-hybridized carbon atoms with outstanding electrical conductivity, high carrier mobility, and a theoretical surface area of 2630 $m^2 g^{-1}$. When coupled with TiO_2 nanoparticles, graphene serves as an electron-accepting and conducting network that extracts photogenerated electrons from TiO_2 and transports them rapidly to the current collector. This charge shuttling effect reduces recombination at TiO_2 surfaces and significantly enhances capacitance under illumination. The large surface area of graphene also improves electrolyte accessibility and provides abundant anchoring sites for TiO_2 nanoparticles, stabilizing the composite structure [10,46]. Reduced graphene oxide (rGO) represents a cost-effective alternative to pristine graphene, retaining much of its conductivity while being more readily available through scalable chemical routes. rGO sheets, decorated with functional groups and residual defects, can form strong interfacial interactions with TiO_2, which improves charge transfer kinetics and enhances structural stability. Moreover, the oxygen-containing functionalities in rGO provide active sites for redox reactions, contributing to pseudocapacitive behavior in addition to improving electron transport. TiO_2/rGO composites have shown higher capacitance values and superior cycling stability compared to bare TiO_2 electrodes, particularly under light irradiation [15]. Carbon nanotubes (CNTs), either single-walled (SWCNTs) or multi-walled (MWCNTs), offer one-dimensional conductive pathways that efficiently transport electrons while also providing mechanical robustness. CNTs can act as nanoscale “wires” that interconnect TiO_2 particles or bind them onto graphene/rGO sheets, creating three-dimensional hierarchical architectures. Such hybrid networks improve electron percolation, reduce resistance at the electrode–electrolyte interface, and enhance rate performance. In addition, CNTs prevent restacking of graphene sheets, ensuring high surface area and effective electrolyte penetration. Studies have shown that TiO_2/CNT composites exhibit improved conductivity by several orders of magnitude compared to pristine TiO_2, enabling higher power densities in supercapacitors and hybrid photoelectrochemical devices [47].

Overall, the incorporation of graphene, rGO, and CNTs into TiO_2 electrodes provides synergistic benefits: (i) significantly improved electrical conductivity through extended conductive networks, (ii) suppression of charge recombination by rapid extraction of photogenerated carriers, (iii) enhancement of specific capacitance due to increased electroactive surface area, and (iv) improved structural integrity under long-term cycling. These hybrid materials represent one of the most effective strategies to overcome the conductivity limitations of TiO_2 and to unlock its potential in photo-supercapacitor applications.

4.2. Synergistic Effects with TiO_2: Interfacial Contact, Defect Mediation, Charge Mobility

The synergistic behavior of TiO_2 when combined with graphene, reduced graphene oxide (rGO), or carbon nanotubes (CNTs) is not a trivial additive effect but arises from the intimate coupling

 doi:10.20944/preprints202511.0205.v1

between the semiconductor and the conductive carbonaceous matrix. Three interconnected mechanisms, as interfacial contact, defect mediation, and charge mobility, play decisive roles in determining the enhanced performance of TiO_2/graphene nanohybrids for photoresponsive supercapacitors. A central factor is the quality of interfacial contact between TiO_2 and graphene-based materials. In bare TiO_2, photogenerated electrons are prone to recombination with holes due to limited electron transport pathways and the absence of efficient sinks. However, when TiO_2 nanoparticles are anchored onto graphene sheets, photogenerated electrons are rapidly injected into the graphene lattice owing to the favorable band alignment between TiO_2 conduction band (–4.5 eV). This strong electronic coupling ensures ultrafast charge separation and electron transfer, thereby suppressing recombination. Cheng et al. demonstrated that TiO_2/graphene nanocomposites show markedly improved photocurrent response compared to bare TiO_2, directly evidencing the role of graphene as an electron acceptor and transport channel [48]. In the context of supercapacitors, this efficient interfacial contact not only prolongs the lifetime of photocarriers but also translates into higher capacitance under illumination, since the additional charges extracted into graphene contribute to double-layer formation and fast surface redox reactions. The second synergistic mechanism involves defect mediation. Defects in TiO_2, such as oxygen vacancies and Ti^{3+} centers, are known to influence electronic conductivity and charge carrier dynamics. While excessive defects promote nonradiative recombination, a controlled defect density can act as shallow traps that extend carrier lifetimes and induce beneficial photodoping. When TiO_2 is coupled with rGO, the residual oxygen functionalities and structural defects of rGO provide nucleation sites for TiO_2 nanoparticle growth, ensuring intimate interfacial contact and stabilization of defect-rich TiO_2 domains. This interaction mitigates detrimental recombination and enhances the persistence of photoinduced doping effects. Chen et al. reported that defect-engineered TiO_2 combined with rGO exhibited a significant decrease in charge-transfer resistance (from ~230 Ω to ~65 Ω) and improved electrochemical capacitance due to enhanced utilization of oxygen vacancies [49,50]. Importantly, graphene sheets help prevent defect collapse during cycling, maintaining the stability of TiO_2's electronic structure. This defect mediation effect is particularly relevant for photo-supercapacitors, where persistent photoconductivity induced by defect states can sustain elevated capacitance even after illumination ceases. A third crucial element is the enhancement of charge mobility through hybridization with conductive carbons. Pristine TiO_2 suffers from intrinsically low electrical conductivity (~10^{-7} S cm^{-1}), which restricts electron transport and reduces power density. Incorporating graphene or CNTs creates highly conductive percolation pathways that dramatically increase the effective conductivity of the composite. CNTs, in particular, act as one-dimensional "wires" that interconnect TiO_2 particles and graphene sheets, forming three-dimensional electron highways. This synergy improves electron percolation, reduces internal resistance, and ensures that photogenerated carriers are rapidly transported to the current collector. Poirot et al. demonstrated that TiO_2/CNT composites achieved a specific capacitance nearly 2.5 times higher than bare TiO_2 electrodes, directly attributable to enhanced electron mobility and improved electrode/electrolyte interface properties [51]. Similarly, hybrid TiO_2/graphene architectures have shown significant reductions in charge-transfer resistance, as confirmed by electrochemical impedance spectroscopy, with values decreasing by more than 60% compared to pristine TiO_2 electrodes [52]. Taken together, these synergistic effects demonstrate that the integration of TiO_2 with graphene, rGO, and CNTs creates hybrid systems where interfacial contact accelerates charge separation, defect mediation stabilizes and harnesses oxygen vacancies, and conductive carbon networks boost charge mobility. This triad of cooperative mechanisms addresses the two major bottlenecks of TiO_2—charge recombination and poor conductivity—while simultaneously enhancing electrochemical capacitance, stability, and multifunctionality. Beyond energy storage, these synergies also underpin the environmental sensing capabilities of TiO_2/graphene systems, as interfacial and defect-mediated charge transfer mechanisms make the electrodes sensitive to adsorbed molecules such as water, oxygen, or volatile organic compounds, which alter capacitance in a measurable and reproducible manner.

 doi:10.20944/preprints202511.0205.v1

In summary, the synergistic integration of TiO_2 with nanocarbon scaffolds transforms a relatively poor electronic conductor into a high-performance photoactive electrode, capable of coupling light harvesting with efficient energy storage and sensing. This cooperative interaction, verified across multiple studies, is a cornerstone in the development of multifunctional photo-supercapacitors for next-generation self-powered devices.

4.3. Common Fabrication Strategies for TiO_2–Graphene Hybrids

The fabrication of TiO_2–graphene hybrids requires methods that ensure intimate interfacial contact, uniform distribution of TiO_2 nanostructures on graphene surfaces, and preservation of the intrinsic conductivity of the carbon scaffold. Several complementary strategies have been developed, each offering specific advantages in terms of morphology control, scalability, and interfacial engineering. One of the most widely adopted routes is the sol–gel method, where titanium alkoxides such as titanium isopropoxide undergo controlled hydrolysis and condensation in the presence of graphene oxide (GO) or reduced graphene oxide (rGO). The oxygen-containing functional groups in GO act as nucleation sites for TiO_2 nanoparticles, ensuring homogeneous deposition and strong interfacial bonding. After subsequent calcination or reduction, uniform TiO_2/rGO nanocomposites are obtained, with well-dispersed nanoparticles anchored on graphene sheets. This method has been successfully employed to produce anatase–graphene composites with improved capacitance and photocatalytic response [53,54]. The hydrothermal/solvothermal synthesis approach is another common strategy, allowing crystallization of TiO_2 under high-pressure and high-temperature conditions in the presence of graphene derivatives. This method produces highly crystalline TiO_2 nanoparticles, nanorods, or nanoflowers anchored on rGO sheets without requiring high-temperature post-treatment. The hydrothermal environment also promotes reduction of GO to rGO, thereby restoring conductivity. Other authors demonstrated that hydrothermally grown TiO_2/rGO hybrids exhibited strong interfacial coupling and enhanced photoelectrochemical performance due to improved crystallinity and conductive pathways [55,56]. In situ reduction–deposition methods offer the advantage of simultaneously reducing GO to rGO and depositing TiO_2 nanoparticles. Chemical reductants such as hydrazine or hydroquinone, or mild thermal treatments, are used to restore the conjugated graphene structure while Ti precursors hydrolyze to TiO_2. This dual process ensures intimate contact and avoids aggregation of TiO_2. Such in situ routes yield composites with excellent electrical conductivity and strong electronic coupling between TiO_2 and rGO [57]. Electrochemical deposition offers an effective way to fabricate TiO_2–graphene hybrids directly onto conductive carbon substrates. In such approaches, graphene-coated electrodes act as templates for TiO_2 film growth, ensuring strong adhesion, precise control over thickness, and enhanced electrochemical stability. For example, Endrődi et al. demonstrated a one-step electrodeposition method in which nanocrystalline TiO_2 films were deposited onto graphene film electrodes. The resulting TiO_2/graphene electrodes exhibited promising photoelectrochemical behavior and notable charge storage capability, outperforming conventional reference materials under similar conditions [58]. More recently, atomic layer deposition (ALD) and chemical vapor deposition (CVD) have been leveraged to build TiO_2–graphene composites with nanoscale precision. ALD enables conformal, ultrathin TiO_2 coatings on graphene/rGO—down to a few nanometers—with excellent coverage and interfacial control; for example, Ban et al. deposited amorphous TiO_2 on high–surface-area rGO via ALD and demonstrated conformal films and improved electrochemical behavior [59]. Likewise, Zhang et al. showed tunable ALD growth of TiO_x on single-layer graphene (uniform amorphous layers at 60 °C vs. ~2 nm nanocrystals at 200 °C after ~20 cycles), directly evidencing the atomic-level control that lowers interfacial resistance and maximizes contact area [60]. In the context of charge storage, Sun et al. anchored ALD-TiO_2 to graphene/CNT electrodes and reported pronounced pseudocapacitive response and cycling stability, underscoring ALD's utility for supercapacitor-oriented hybrids [61]. Complementarily, CVD routes have been used to integrate TiO_2 with graphene while controlling crystallinity and film continuity; recent overviews explicitly survey CVD as a viable pathway within TiO_2/graphene composite synthesis toolkits [62]. Additional ALD studies on TiO_2–

 doi:10.20944/preprints202511.0205.v1

graphene further corroborate conformal coverage and thickness control for optimizing electrochemical interfaces [63].

In summary, fabrication strategies for TiO_2–graphene hybrids range from solution-based approaches such as sol–gel and hydrothermal synthesis to advanced thin-film techniques such as ALD and CVD. Each method offers unique advantages: sol–gel ensures molecular-level mixing, hydrothermal routes yield high crystallinity and morphological control, in situ reduction provides strong interfacial bonding, electrochemical deposition enables scalable integration on electrodes, and ALD/CVD deliver precise nanoscale architectures. Rational selection of synthesis strategies, often involving combinations of these methods, is essential for designing high-performance TiO_2–graphene electrodes optimized for photoresponsive supercapacitors.

4.4. Examples of Enhanced Electrochemical Performance in Hybrids

Multiple, independently verified studies show that coupling TiO_2 with nanocarbon (graphene, rGO, CNTs) reliably boosts capacitance, rate handling and durability—often adding photo-responsiveness that further elevates performance. A representative early benchmark is the rGO–TiO_2 study by Xiang et al., who compared TiO_2 nanobelts (NBs) vs nanoparticles (NPs) anchored on reduced graphene oxide. At an rGO:TiO_2 mass ratio of 7:3, rGO–TiO_2 nanobelts delivered 225 F g^{-1} (0.125 A g^{-1}), whereas the rGO–TiO_2 nanoparticles reached 62.8 F g^{-1}, evidencing the advantage of anisotropic TiO_2 morphologies when intimately interfaced with conductive graphene [64]. To minimize interfacial resistance and preserve electron pathways, laminated "sandwich" electrodes place TiO_2 between rGO sheets. Ramadoss et al. built a porous rGO/TiO_2-nanorod/rGO laminate that reached 114.5 F g^{-1} (5 mV s^{-1} in 1 M Na_2SO_4) and retained >85% capacitance after 4000 cycles—performance attributed to efficient ion access and short electron paths through the rGO framework [65]. Flexible layered films further highlight the utility of rGO as both a current collector and spacer to suppress graphene restacking. Kim et al. prepared stacked rGO/TiO_2 films by vacuum filtration; the composites delivered 286 F g^{-1} at 1 A g^{-1}, ≈93% retention after 1000 cycles, and device-level energy/power densities of ≈39.7 Wh kg^{-1} and ≈472 W kg^{-1} in a symmetric cell—figures difficult to reach with TiO_2 alone [66]. ALD offers another validated route: ultrathin, conformal TiO_2 grown directly on high–surface area carbon can switch on robust intercalation-type pseudocapacitance while keeping diffusion lengths short. Sun et al. anchored amorphous TiO_2 films to graphene aerogels (and CNTs) via ALD and observed specific capacitances of ~97.5 F g^{-1} (graphene) and ~135 F g^{-1} (CNTs) at 1 A g^{-1} after 50 ALD cycles—well above the parent carbons—along with good cycling and an asymmetric device operating to 1.5 V in aqueous KOH [61]. Three-dimensional scaffolds that co-embed TiO_2 and graphene also deliver strong gains by combining abundant ion-accessible porosity with conductive highways. Jiang et al. used a loofah-derived, 3D hierarchical carbon as a host for graphene and TiO_2; the best composite reached 250.8 F g^{-1} at 2 A g^{-1} with decent rate performance and >80% retention over 100 cycles [67]. When the objective is an integrated photo-supercapacitor rather than a stand-alone electrode, coupling a TiO_2 photoanode with a graphene-based capacitor can preserve charge during light-off periods and reduce series resistance at the junction. In a three-electrode integrated device that paired a dye-sensitized TiO_2 photoanode with a PPy/rGO symmetric supercapacitor, Lau et al. measured 124.7 F g^{-1} specific capacitance and 70.9% retention after 50 charge–discharge cycles under 100 mW cm^{-2} illumination [68]. The same design principles extend to other nanocarbon partners. For example, coating multi-walled carbon nanotubes (MWNTs) with TiO_2 nanodots (binder-free) produced high areal capacitance with strong rate capability, emphasizing that intimate, conformal TiO_2–carbon contact—not just the carbon type—governs performance [69]. Across these examples, several consistent, mechanism-level features explain the gains: (i) rGO/graphene provides fast, percolating electron pathways that mitigate TiO_2's low conductivity; (ii) conformal or laminated architectures shorten $Li^+/H^+/Na^+$ diffusion paths in TiO_2 and maximize electrochemically active surface; (iii) interfacial defect states and heterojunctions at TiO_2–graphene contacts suppress charge recombination and promote faradaic storage; and (iv) 3D porosity and flexibility (films/hydrogels) maintain electrolyte access under practical deformation or high current

 doi:10.20944/preprints202511.0205.v1

loads. Together, these effects lift specific/areal capacitance, preserve capacity at high rates, and enhance cycling life—while in integrated photo-supercapacitors, TiO_2's photoactivity can directly assist charging under illumination. Building on the preceding discussion of interfacial contact, defect mediation, and charge-transport pathways, it is helpful to ground these concepts in a concrete dataset before moving on. As a performance example of nanocarbon-assisted TiO_2 electrodes, Figure 2 summarizes cyclic voltammetry (CV), galvanostatic charge–discharge (GCD), cycling stability, and rate capability for bio-carbon/graphene/TiO_2 composites, highlighting how the carbon framework translates into measurable gains in charge storage and durability [67].

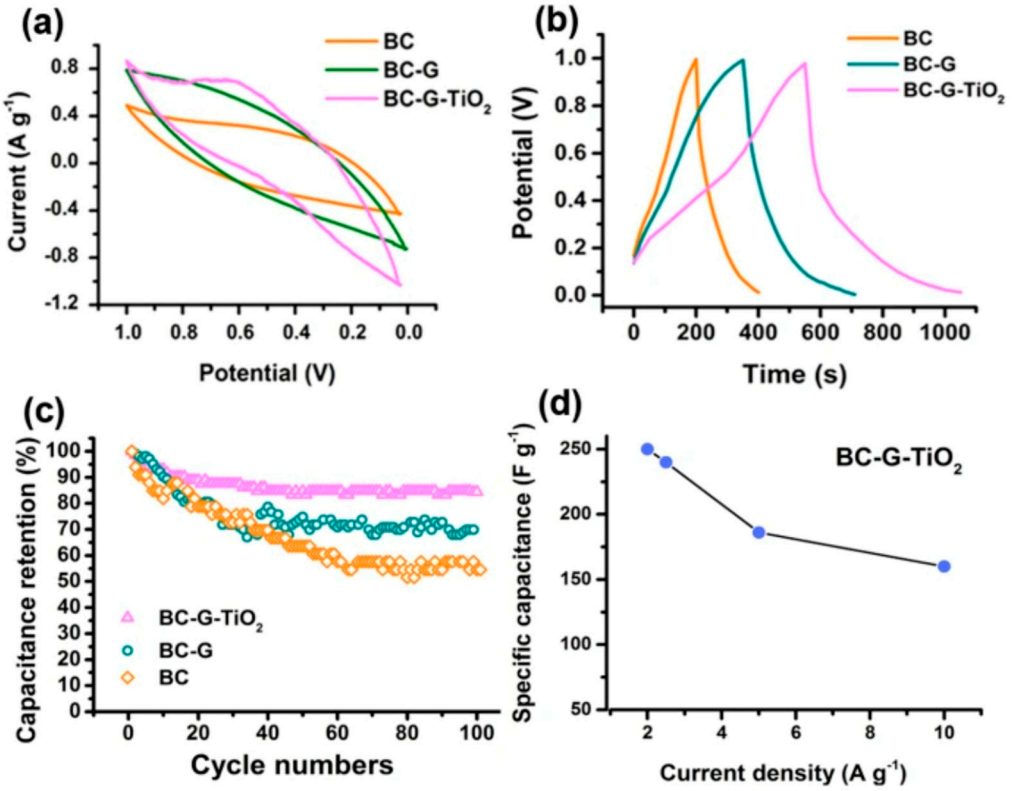

Figure 2. Electrochemical performance of bio-derived carbon–graphene–TiO_2 composite electrodes: (a) cyclic voltammetry (10 mV s^{-1}), (b) galvanostatic charge–discharge curves, (c) cycling stability at 2 A g^{-1}, and (d) specific capacitance vs. current density, highlighting the synergistic enhancement of graphene/carbon with TiO_2. (Adapted with permission from ref. [67], Springer Nature 2018).

5. Dual-Functionality: Energy Storage + Environmental Sensing

5.1. Principles of Capacitive Sensing: VOCs, Humidity and Gases

Capacitive sensing is fundamentally based on the modulation of dielectric properties and interfacial charge dynamics in response to external environmental stimuli. A capacitor consists of two conductive electrodes separated by a dielectric medium; when the dielectric constant or conductivity of this medium changes due to the adsorption of volatile organic compounds (VOCs), water molecules, or gaseous species, the capacitance is altered. This variation provides a direct transduction pathway for sensing. In supercapacitor-based systems, the electrodes already display high surface area and tunable surface chemistry, which can be exploited not only for charge storage but also for environmental detection. In the case of humidity sensing, the mechanism is primarily governed by the adsorption and desorption of water molecules at hydrophilic sites on the electrode or electrolyte interface. At low relative humidity, chemisorption dominates, with water molecules binding strongly to defect sites or oxygen-containing functional groups. As humidity increases, multilayer physisorption occurs, leading to the formation of a continuous water layer. This enhances proton

 doi:10.20944/preprints202511.0205.v1

conduction and dielectric polarization, thereby significantly modulating the capacitance response [70]. For VOC detection, the principle involves changes in the dielectric constant of the medium surrounding the active electrode surface. Polar VOCs (e.g., ethanol, acetone) interact strongly with functional groups or porous frameworks, producing measurable capacitance variations. By tailoring electrode materials—such as incorporating graphene, metal oxides, or MXenes—the sensitivity and selectivity toward specific analytes can be enhanced. In particular, MXene-based electrodes show strong binding affinity for polar molecules due to surface-terminated functional groups such as –OH and –F, which makes them highly attractive for dual energy-storage and sensing platforms [71]. Gas sensing, especially for small molecules such as NH_3, CO_2, or NO_2, is mainly governed by adsorption-induced charge transfer and polarization effects. The adsorption of electron-donating or electron-withdrawing gases modifies the interfacial charge distribution at the electrode, which can shift the local Fermi level and alter both double-layer capacitance and capacitance in porous frameworks. This behavior has been widely reported for two-dimensional materials such as graphene, where surface functionalization enables room-temperature NH_3 detection through specific electronic interactions with functional groups [72]. For CO_2 detection, copper oxides and their derivatives exhibit strong potential as active sensing materials, since the adsorption of CO_2 molecules modifies the work function and surface states, leading to measurable capacitance changes under room-temperature conditions with low energy consumption [73]. Similarly, NO_2 detection has been associated with the strong interaction of this oxidizing gas with surface defects or vacancies in semiconducting and photoactivated materials, which induces charge transfer and capacitance modulation. Photoactivated materials such as TiO_2, WO_3, or hybrid structures have shown fast and sensitive responses to low NO_2 concentrations under ambient conditions [74].

Integrating these capacitive sensing mechanisms into supercapacitors enables the development of dual-functionality devices: systems capable of simultaneously storing electrical energy while acting as responsive sensors for environmental monitoring. This multifunctionality represents an emerging paradigm in the field of "smart supercapacitors" designed for the Internet of Things (IoT), where energy storage elements also serve as active sensing nodes.

5.2. Case Studies of TiO_2 or Graphene-Based Capacitive Sensors

Early thin-film TiO_2 devices established what makes capacitive humidity sensing so compelling: enormous dynamic range at room temperature and fast, repeatable response. Using glancing-angle deposition (GLAD), Steele, Brett and co-workers coated interdigitated electrodes (IDEs) with nanocolumnar TiO_2 and observed capacitance rising from ~1 nF to ~1 μF as RH increased from 2 % to 92 %, a hallmark of interfacial and dielectric-constant modulation in highly porous oxides. Their IEEE letter highlighted sub-second dynamics, while a follow-up study quantified ~270 ms response using similar GLAD films; critically, performance could be photocatalytically regenerated under UV after surface fouling—an early demonstration of self-cleaning in capacitive sensors (see Table 1, rows 1–3) [75]. Graphene-family dielectrics translate the same capacitive principle to 2D materials. Graphene oxide (GO), laminated over IDEs, behaves as a hygroscopic, nanolaminate dielectric whose permittivity and interfacial polarization rise with water uptake. Practical device builds report strong, frequency-dependent capacitance changes at room temperature and straightforward microfabrication. For instance, GO capacitors fabricated on common CMOS-style IDEs show large RH transfer functions across the ambient range, and GO/Ag-nanoparticle composites layer-by-layer onto IDEs achieve exceptionally high capacitance sensitivity (see Table 1, rows 4–5) [76]. Beyond humidity, graphene varactors enable *gas* sensing by exploiting quantum capacitance. Adsorbates shift graphene's Fermi level, changing the series combination of geometric and quantum capacitance. A canonical wireless vapor sensor coupled a metal-oxide-graphene varactor to an inductor and read humidity as a linear resonant-frequency shift of ~5.7 kHz per %RH over 1–97 % RH, cleanly tying the signal to quantum-capacitance modulation. Related work used graphene varactors to capacitively detect intercalated water between graphene and HfO_2, confirming rapid, reversible, room-temperature operation—useful design cues for capacitive gas sensing generally (Table 1, rows 6–7)

 doi:10.20944/preprints202511.0205.v1

[77]. Finally, recent NO_2 studies show that capacitive readout is not restricted to water vapor. Using CVD graphene with an enhanced geometrical capacitance back-gate stack, researchers measured capacitance changes tracking 1–100 ppm NO_2 at room temperature, explicitly attributing the signal to quantum-capacitance effects in graphene. This anchors feasibility for ppm-level, room-temperature capacitive gas sensors, complementing the humidity literature (Table 1, row 8) [78]. As summarized in Table 1, these case studies collectively map the design space, porous TiO_2 dielectrics for large RH dynamic range and self-regeneration; GO (and GO-nanocomposites) for CMOS-friendly, high-sensitivity capacitive humidity transduction; and graphene varactors for quantum-capacitance-based humidity and gas detection at room temperature. Building on the device-level considerations above, it is useful to anchor the discussion with a frequency-tuned capacitive sensing example based on CVD graphene. To that end, Figure 3 combines the device schematic and measurement configuration with representative performance metrics, linking architecture and readout to practical sensing outcomes. Specifically, the composite figure assembles the layout and measurement window together with dynamic response traces and the corresponding calibration curve for NO_2, illustrating how adsorption-induced doping modulates the measurable capacitance in a controlled frequency band.

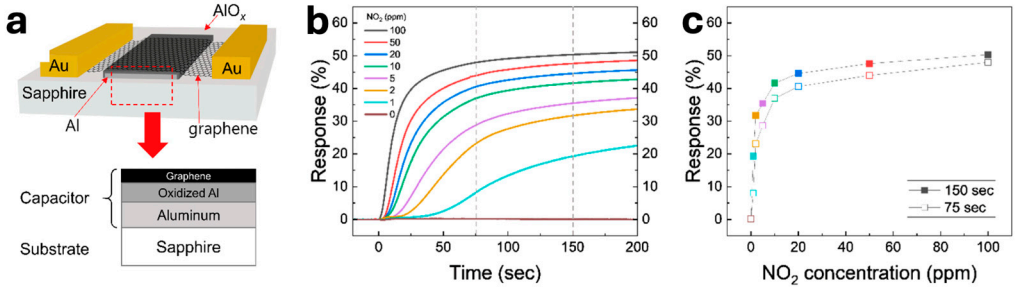

Figure 3. CVD-graphene capacitive NO_2 sensor: (a) device schematic and measurement configuration (frequency-tuned capacitance readout); (b) dynamic response/recovery traces under stepwise NO_2 exposure at increasing concentrations; and (c) calibration of the capacitive response versus NO_2 concentration at fixed exposure times, highlighting linearity and LOD. (Adapted with permission from ref. [78], MDPI 2023).

Table 1. Representative TiO_2- and graphene-based capacitive sensors: materials, configuration, analyte, performance and mechanism.

Material/Structure	Analyte	Configuration	Performance	Mechanism	References
Sputtered TiO_2 thin films	Humidity	Capacitive IDE	Broad RH response, stable signals	Water adsorption on hydroxylated TiO_2 surfaces, proton conduction	[79]
TiO_2 “micro-flowers”	Humidity	Capacitive thin film	High sensitivity across wide RH, fast response/recovery	Hierarchical porosity, large surface area, strong adsorption sites	[80]
TiO_2 QDs / N-MWCNTs	Humidity	Capacitive composite	Strong signals at low RH, high stability	Quantum confinement, CNT conductivity, enhanced adsorption	[81]
Graphene oxide films	Humidity	Capacitive IDE	Ultrahigh sensitivity (~37,800%), wide RH range	Multilayer water adsorption, swelling, dielectric constant change	[82]

 doi:10.20944/preprints202511.0205.v1

Reduced graphene oxide films	Humidity	Capacitive IDE	Fast response, moderate sensitivity	Improved conductivity, reduced hysteresis	[76]
TiO_2/GO nanocomposite	Humidity	Flexible capacitive/resistive	Response < 1 s, recovery < 1 s, low hysteresis (~4%)	Synergy: GO hydrophilicity + TiO_2 adsorption, stable mechanics	[83]
Graphene–TiO_2 heterostructure	Humidity / gases	Layered composite	Enhanced selectivity, amplified response	Charge transfer at graphene–TiO_2 interface, defect engineering	[84]
GO/TiO_2 optical hybrid	Humidity	Optical + capacitive	Ultra-sensitive, wide dynamic range	Optical interference + dielectric modulation	[85]

5.3. Mechanisms of Analyte Interaction and Change in Capacitance

This section examines the mechanisms by which analytes modulate the measured capacitance in porous and low-dimensional electrodes engineered to serve concurrently as environmental sensors. In capacitive transduction, three interrelated pathways are predominant: (i) bulk and interfacial dielectric polarization within the sensing layer; (ii) ionic transport and electrical double-layer phenomena in saturated pores and at electrolyte–solid interfaces; and (iii) alterations of the electronic density of states—i.e., quantum capacitance—in materials such as graphene. The relative contribution of each pathway is governed by the electrode material (e.g., TiO_2 versus graphene/GO), the excitation frequency, the ambient humidity, and the applied bias conditions. At the lowest humidities, H_2O chemisorbs on oxide surfaces (e.g., TiO_2) to form surface hydroxyls; as RH rises, physisorbed water layers build up and percolate. The film's effective permittivity increases and an interfacial (Maxwell–Wagner–Sillars, MWS) polarization emerges at boundaries between grains/pores and the adsorbed electrolyte, boosting the measured capacitance of interdigital or sandwich structures, especially at kHz–MHz where dipolar and space-charge relaxations are active. The same progression also enables protonic Grotthuss transport along water networks, further lowering impedance and amplifying the capacitive signature. These mechanisms—and their frequency dispersion and hysteresis—are well established in humidity-sensor reviews and dielectric spectroscopy of composites [70,86,87]. In nanostructured TiO_2 (columns/chevrons made by GLAD), capillary condensation and ultrahigh surface area magnify both permittivity changes and MWS effects, yielding large $\Delta C/\Delta RH$ and sub-second dynamics. Importantly, TiO_2's photocatalysis under near-UV can "self-regenerate" the surface by oxidizing foulants and restoring hydroxyl chemistry, one reason GLAD TiO_2 capacitive RH sensors maintain stability without heaters [75,88–90]. For graphene and graphene oxide, two additional levers appear. First, GO swells and uptakes water, and its effective dielectric constant rises strongly with RH; both the volumetric water fraction and interlayer spacing control permittivity and, thus, the capacitance seen by interdigitated electrodes or microwave resonators. Ultrafast GO humidity sensors (tens of milliseconds) arise from GO's "superpermeability" to water and rapid sorption/desorption kinetics [82,91]. Second, and unique to graphene, is quantum capacitance (Cq)—the contribution from its low electronic density of states. When analyte adsorption donates or withdraws charge (e.g., NO_2 as a strong acceptor), the Fermi level and DOS shift, changing Cq; since the measured capacitance is $1/C_{tot}=1/C_{geom}+1/C_q$, even modest DOS changes can be read out as ΔC. This has been directly measured in graphene and exploited in varactor-based chemicapacitors and passive wireless resonators whose frequency follows humidity or gas concentration via Cq [92–95]. Gas molecules interact by physisorption or weak chemisorption with graphene and many oxides, producing adsorption-induced charge transfer and local polarization. On graphene, single-molecule events alter carrier density and, consequently, Cq (and conductance), with strong p-doping by NO_2 and weaker n- or p-doping for NH_3, CO, and H_2O

 doi:10.20944/preprints202511.0205.v1

depending on coverage and defects. These donor/acceptor trends are established by single-molecule detection experiments and first-principles studies [96,97]. When these sensing films are integrated into electrochemical capacitors, a further channel couples in: EDL formation and ion transport within flooded pores. Analytes that change the ionic strength, pH, viscosity, or surface charge (e.g., by deprotonating/adding hydroxyls) shift the EDL capacitance and its characteristic RC times. Porous electrodes therefore convert subtle changes in local electrolyte chemistry into measurable ΔC and phase shifts in impedance spectra; frequency helps disentangle dielectric/MWS processes (higher f) from diffusion/EDL processes (lower f) [1,98]. Pulling these pieces together suggests a practical picture for TiO_2 and graphene/GO sensors:

- In TiO_2, ΔC is dominated by changes in dielectric permittivity (water uptake), MWS interfacial polarization, and (under UV) photocatalytic surface rejuvenation that resets hydroxyl chemistry, ideal for low-power, room-temperature RH sensing with regeneration instead of heaters [89].
- In GO films, swelling + permittivity increase control ΔC at low–mid frequencies, while fast sorption kinetics enable rapid response; at GHz, the humidity-dependent complex permittivity can also be read wirelessly [91].
- In graphene varactors, adsorption-induced doping perturbs Cq, enabling capacitive readout of water and certain gases, even wirelessly, without needing high temperatures [77].

Two caveats matter for devices that co-store energy while sensing. First, bias history (state of charge) sets the operating Fermi level and the fraction of C_{tot} coming from Cq vs. geometric/EDL, so the same analyte can cause different ΔC at different biases. Second, analyte-driven capillary condensation and electrolyte uptake can transiently raise capacitance but also introduce hysteresis and drift, mitigated by porous architectures that favor fast desorption and, in TiO_2, by UV regeneration [87,88].

5.4. Design Criteria for Integrating Sensing and Storage in a Single Device

Integrating environmental sensing into a supercapacitor is a co-optimization problem: the architecture must sustain large, reversible charge storage while transducing small analyte-induced changes into a stable capacitance signal. The first decision is which physical channel carries the sensing signal—(i) dielectric/interfacial polarization in a porous film, (ii) ion/EDL processes in flooded pores, or (iii) quantum-capacitance modulation in low-DOS materials such as graphene—because that choice fixes geometry, readout frequency, and bias regime. Authoritative reviews map the dielectric humidity mechanisms [70,87], while porous-electrode charging and desalination physics frame the EDL regime [98]. The quantum-capacitance lever in graphene has been measured directly [95]. With the transduction pathway chosen, morphology is the dominant handle to reconcile sensing and storage. Hierarchical porosity (micro/meso/macro) allows fast analyte ingress and desorption (sensing) while preserving high double-layer capacitance (storage). Classic EDLC guidance shows that capacitance is maximized when pore size closely matches ion size, providing a practical target for carbon/ion couples [99], and broader design trade-offs on pore architecture and electrolytes are summarized by Simon & Gogotsi [1]. In thin-film dielectrics (e.g., GLAD TiO_2, laminated GO), thickness and tortuosity set the balance: thicker, more open structures yield larger permittivity swings but slower wash-in/wash-out; thinner films respond faster but with smaller ΔC [99]. A robust integration also separates sensing from storage in the electrical domain. Measuring at kHz–MHz emphasizes dielectric/Maxwell–Wagner polarization (sensing), whereas low-frequency EIS resolves EDL/pseudocapacitive storage—so the same device can be interrogated in different bands with minimal cross-talk. Operating-point control then reduces interference: oxide/GO capacitive sensors are usually read near open-circuit to minimize leakage; graphene varactors are biased near the Dirac region where dC_q/dE_F is high [95]. For devices that sense during idle windows between charge/discharge pulses, this spectral and temporal partitioning leaves energy throughput

 doi:10.20944/preprints202511.0205.v1

largely undisturbed [98]. Electrolyte and interface choices must serve both functions. High-voltage, high-conductivity electrolytes favored for storage can screen interfacial fields or introduce their own humidity response; conversely, highly hygroscopic solvents may swamp an RH signal. Practical designs select electrolytes (or solid/gel analogues) that are stable, low-volatility, and compatible with the target analyte, and use impedance spectra to separate high-frequency dielectric changes from low-frequency EDL shifts [1,98]. Surface chemistry should be tuned for reversible adsorption; in TiO_2, near-UV photocatalysis can periodically regenerate the sensing surface without heaters, preserving long-term stability alongside storage cycling [89]. Finally, packaging and readout complete the design. Selective, breathable windows or membranes localize analyte access to the sensing region while protecting current collectors and electrolyte headspace; co-located temperature/RH references or a second frequency channel help compensate cross-sensitivities. For ultralow-power operation and remote interrogation, passive LC tags coupled to graphene varactors are attractive: a canonical implementation reported a linear ~5.7 kHz per %RH resonant-frequency shift from 1–97 % RH at room temperature, directly tied to quantum-capacitance modulation [77]. Designs following this workflow—mechanism choice → morphology → frequency/bias partition → electrolyte/interface → packaging—most reliably deliver truly dual-functional supercapacitors that store energy while sensing their environment in real time.

5.5. Stability, Selectivity, and Signal Resolution Challenges

Integrating sensing with electrochemical storage exposes the sensor to moisture, gases, electrolytes, and cycling biases that can compromise stability, blur selectivity, and limit signal resolution. Here we outline the main degradation pathways and practical mitigation strategies, then discuss how to preserve analyte specificity and push the noise floor low enough for meaningful limits of detection.

Stability: In oxide dielectrics (e.g., TiO_2), long-term drift often arises from surface fouling and slow changes in hydroxyl chemistry; in layered carbons (GO), repeated sorption/desorption can induce swelling, interlayer rearrangement, and minor delamination, producing baseline shifts and humidity hysteresis. A robust countermeasure for TiO_2 is photocatalytic self-regeneration under near-UV, which oxidizes organic foulants and restores the hydrophilic surface without heaters—a strategy demonstrated on glancing-angle-deposited (GLAD) TiO_2 IDE capacitive sensors and shown to recover sensitivity after aging. In practice, brief UV pulses scheduled between storage cycles can reset the sensing surface with negligible energy overhead [89]. GO-based capacitive RH sensors are prized for their speed, but require attention to hysteresis and drift control. Ultrafast GO devices (ms–100 ms transients) leverage the material's "superpermeability" to water; however, the same rapid uptake can leave residual water in galleries, shifting the baseline unless the film is thin, well-anchored, and interrogated at frequencies that minimize slow space-charge contributions. Practical remedies include using thinner GO laminates, mild thermal or UV conditioning cycles, and referencing at a secondary frequency [82,91]. Graphene varactors add a different stability consideration: adsorption shifts the Fermi level and therefore the quantum capacitance; stable baselines demand clean, well-passivated oxides and minimized interfacial water. Mechanistic work directly visualized intercalated H_2O between graphene and HfO_2 and showed the associated capacitance changes are fast and reversible—useful for sensing, but also a reminder that device stacks must control buried interfaces to avoid slow drift [92].

Selectivity: Capacitive sensors are inherently sensitive to multiple stimuli (RH, temperature, pressure, co-adsorbed gases) because many of these modulate permittivity or carrier density. Selectivity can be improved along three axes. *(i) Materials/chemistry:* introduce functional groups or defect motifs that preferentially bind the target (e.g., strong acceptors like NO_2 on graphene); literature on gas adsorption on graphene establishes donor/acceptor trends that map to predictable Fermi-level shifts. *(ii) Architecture:* include differential channels—an active sensor and a reference shielded from the analyte or functionalized for an orthogonal response—and subtract them in hardware/firmware. *(iii) Frequency/bias domain:* use multi-frequency interrogation to separate

 doi:10.20944/preprints202511.0205.v1

dielectric (kHz–MHz, Maxwell–Wagner) from EDL/diffusive processes (Hz–tens of Hz), and choose a bias where the analyte pathway has a large derivative (e.g., near the Dirac region for graphene varactors). Comprehensive reviews of humidity transduction and interfacial polarization provide the physics and compensation playbook; classic graphene studies map gas-induced doping [86,87,97].

Signal resolution (noise, LOD, dynamic range): The minimum resolvable ΔC (or Δf in resonant tags) is set by a combination of dielectric noise (thermally driven polarization fluctuations), instrumentation noise (front-end amplifier, ADC), and 1/f processes associated with slow adsorption/desorption or charge trapping. Two pragmatic levers consistently help. *(i) Encode C as frequency* using an LC resonator or oscillator: frequency can be tracked with high precision at μW-level power, and the slope can be engineered—graphene varactor tags report a linear ~5.7 kHz per %RH over 1–97 %RH at room temperature, allowing sub-%RH resolution with simple readers. *(ii) Use short time-gated interrogations between charge/discharge pulses (for integrated supercapacitors) to avoid load-transient noise and let the sensor relax. Mechanistic studies of quantum capacitance in graphene validate that biasing near the Dirac point maximizes dC_q/dE_F, improving SNR for small coverage changes [77,95].

Implications for dual-function devices: When sensing shares the electrode/electrolyte with storage, calibration should be embedded in the operating routine: (1) a brief high-frequency sweep to extract the dielectric signature, (2) a low-frequency EIS point to confirm storage health (EDL/pseudocapacitance), and (3) a reference channel or secondary frequency to regress out temperature and ambient RH. Where compatible with the chemistry, UV refresh (TiO_2) or short conditioning cycles (GO) control drift without thermal budgets that would hurt cycle life. In graphene stacks, controlling buried water and oxide traps at the varactor interface is essential to keep quantum-capacitance transduction stable over months. Together, these tactics preserve stability and selectivity while keeping the noise floor low enough to resolve the small capacitance changes that encode analyte information [87,92].

6. Device Architectures and Performance Metrics

6.1. Asymmetric vs. Symmetric Configurations

From a device standpoint, the architecture determines not only how charge is stored, but also the voltage a cell can safely sustain, how quickly it can deliver that charge, and how reproducibly those figures can be reported. Symmetric cells (classically carbon‖carbon EDLCs) prioritize low internal resistance, near-ideal triangular galvanostatic traces, and long cycle life. By contrast, asymmetric cells pair dissimilar electrodes (e.g., a faradaic/pseudocapacitive positive with a carbon negative) so that each works within its own stable potential sub-window; the combined window then lifts the full-cell voltage and, via $E=1/2C_{cell}V^2_{cell}$, the attainable energy at comparable cell capacitance. A comprehensive treatment of the design logic, materials families, and performance evaluation for asymmetric supercapacitors is given by Shao and co-workers [100]. Electrolyte choice largely fixes the voltage window for symmetric EDLCs. In aqueous media, practical operation remains near ~1.0–1.2 V because of water stability (kinetics and surface chemistry set the exact limit), whereas water-in-salt (WIS) electrolytes widen the aqueous stability window toward ~2–3 V, narrowing the historical gap to organic systems while preserving safety. A focused review of WIS for supercapacitors summarizes mechanisms, salt systems, and device data [101], and carbon‖carbon demonstrations around ~2.0–2.4 V exemplify the trend [102]. The principal attraction of asymmetry is that it lifts V_{cell} without abandoning supercapacitor-class power. Practically, assembling such cells requires charge balancing so the two electrodes reach their limits simultaneously. This is codified by the standard mass-balance relation:

$$\frac{m_+}{m_-} = \frac{C_- \Delta V_-}{C_+ \Delta V_+}$$

 doi:10.20944/preprints202511.0205.v1

with C± the specific capacitance (measured in each electrode's operating sub-window ΔV±). Recent analyses formalize this rule and discuss how it should be applied at the intended current density and scan rate [103], and many device papers state it explicitly in their methods/Supplementary Material. Because architecture influences how metrics are extracted, methodology matters. For comparability across the literature, cell capacitance, energy, and power should be derived from two-electrode device data, reserving three-electrode measurements for mechanistic screening; this distinction, and common pitfalls that inflate apparent performance, were laid out in a widely adopted best-practice paper [104]. Finally, power and lifetime trade off differently in the two schemes. Symmetric carbon cells typically exhibit the lowest ESR and the most robust cycling; asymmetric cells inherit extra charge-transfer and diffusion resistances from the faradaic side, occasionally introducing mild plateaus at high load. Modern designs mitigate these effects through conductive scaffolds, nanostructuring, and careful mass balancing, yet the key advantage remains: by distributing the operating potential across complementary electrodes, asymmetric architectures deliver higher usable V_{cell} (and thus energy) while retaining the fast-charge character that distinguishes supercapacitors. For an expanded discussion of these trade-offs and reporting conventions, see Shao *et al.* [100] together with the WIS and best-practice references cited above.

6.2. Flexible, Wearable, and Micro-Supercapacitor Formats

Flexible and wearable supercapacitors—and their microscale cousins designed for on-chip use—share a common goal: high power and robust cycle life in form factors that bend, stretch, and shrink to millimetre or even micrometre footprints. The field matured from early on-chip, interdigital devices based on carbide-derived carbon and onion-like carbon, which established the volumetric and frequency benchmarks that later flexible formats would try to match or exceed [105,106]. Soon after, ultrathin planar graphene supercapacitors [107] and laser-scribed graphene [108,109] showed that microsupercapacitors (MSCs) could be patterned directly onto flexible polymer sheets, retain rapid RC time constants, and survive mechanical deformation. These canonical demonstrations defined today's design space for flexible and wearable power: planar in-plane electrodes for high rate and compact packaging, solid or gel electrolytes to prevent leakage, and mechanically compliant current collectors and encapsulants. From a fabrication perspective, three families dominate. First, lithography-compatible thin-film routes (CDC, OLC, multilayer graphene) deliver high volumetric figures and wafer-level integration, but require clean-room tooling. Second, direct laser writing, most famously, laser-scribed graphene, patterns conductive, porous carbons rapidly over large flexible substrates without inks or binders, enabling arrays and circuit-level integration in minutes. Third, additive printing (screen, inkjet, aerosol jet, 3D) is now a mainstream path to MSCs, with comprehensive reviews mapping printable inks, interdigitated geometries, and device-level metrics [110,111]. Collectively these strategies trade maximum performance for throughput and mechanical compliance, letting researchers tune toward either areal power (dense interdigital fingers, short ion paths) or volumetric energy (thicker, hierarchical films). All-solid-state flexible MSCs pioneered the recipe most wearables still use: micro-patterned carbon or oxide films on polyimide (or PET), infiltrated with a quasi-solid PVA-acid/alkali gel (e.g., PVA/H_3PO_4), then encapsulated. A widely cited early example is "An All-Solid-State Flexible Micro-Supercapacitor on a Chip" [112], followed by multilayer-graphene arrays on plastic that combine high power with bendability. The solid-state gels suppress leakage and enable ultrathin, cut-and-mount form factors for integration near sensors, antennas, or microcontrollers without package penalties. Stretchability, beyond mere flexibility, comes from structural mechanics as much as from materials. Early stretchable MSC arrays used serpentine interconnects and elastomeric substrates to achieve biaxial strain without compromising areal coverage [113,114]. Laser-patterned and kirigami-inspired layouts later added large, reversible strain ranges while keeping the electrodes contiguous [115]. These architectures now underpin "skin-like" power modules that can laminate onto soft robotics or e-textiles and maintain capacitance under bending, twisting, and 20–50% tensile strain. Wearable formats also migrate from sheets to fibers. Fiber- and yarn-shaped supercapacitors weave directly into textiles, leveraging coaxial or twisted

 doi:10.20944/preprints202511.0205.v1

core–shell electrodes with gel electrolytes. A representative milestone coupled carbon/MnO_2 core–shell fibers into all-solid devices [116], while recent assessments make clear that state-of-the-art fiber supercapacitors already meet or exceed the instantaneous power needs of most wearables, and many approach the required areal/volumetric energy densities [117]. In practice, textile integration shifts the bottleneck from electrode kinetics to packaging: washability, sweat/ion ingress, and repeated crumpling demand breathable yet hermetic barriers and mechanically matched encapsulants.

Materials innovations continue to push performance at small footprints. Graphene remains the workhorse for laser and printed MSCs; MXenes (e.g., $Ti_3C_2T_x$) add metallic conductivity and high volumetric capacitance, enabling dense on-chip reservoirs and even stretchable MXene MSCs via crumpled or serpentine patterns [118]. Additive manufacturing of MXene inks and aerosol-jet or 3D-printed microelectrodes further blurs the line between rigid, flexible, and stretchable platforms, allowing heterogeneous integration with sensors, microcontrollers, and antennas on the same substrate. Electrolytes and encapsulation are as decisive as electrodes. Hydrogel and ionogel electrolytes (PVA-acid/alkali, polymerized ionic liquids, “water-in-salt” gels) widen temperature windows, raise safe operating voltages in solid-state stacks, and improve interfacial wetting under strain, all key for wearables. A recent survey highlights how hydrogel chemistries (conducting-polymer and biopolymer gels) trade conductivity, stretchability, and self-healing against processability and moisture control in garments [119]. For microdevices, thin, conformal encapsulation (parylene, ALD oxides, fluoropolymers) minimizes vapor-phase drift without throttling ion transport across microgaps—critical to preserve the fast frequency response that sets MSCs apart from microbatteries.

Finally, the most compelling demonstrations combine form factors. Printed MSC arrays on plastics or fabrics can power sensors and radios directly or buffer intermittent energy harvesters (e.g., triboelectric and photovoltaic textiles). Laser-scribed graphene MSCs tiled into circuits provide line-filtering-class frequency response in small footprints, while printed MSC arrays have recently withstood hundreds of wash cycles and elevated temperatures, pointing to industrially relevant reliability [1][108,120]. The convergence of these approaches (wafer-level microfabrication for density, laser/printing for scale and compliance, and soft-matter electrolytes for safety) now defines a practical path to unobtrusive, skin- and fabric-integrated energy storage.

6.3. Photonic Stimulation Setups (Solar, LED, Laser-Assisted)

For supercapacitors that also “listen” to their surroundings, light is a surprisingly versatile control knob. In practice it acts along three intertwined routes. First, photocharging/photocapacitance: illumination generates carriers in a photoactive layer (or in a coupled photovoltaic unit) and that extra charge is stored electrostatically or pseudocapacitively. Second, photothermal assistance: light gently heats the electrode–electrolyte microenvironment, lowering ionic and charge-transfer resistances so the same device looks faster and less resistive. Third, laser-enabled microfabrication: short pulses write, reduce, or heal porous micro-architectures that later behave as high-rate capacitors. A recent, comprehensive framework sets common language for these modes—device topologies, figures of merit, and testing under standard irradiance (AM1.5G, 100 mW cm^{-2})—which we adopt here [121]. Solar coupling now appears in two flavors that are easy to tell apart on the bench. In monolithic photo-supercapacitors, the light-harvesting and storage functions share materials or layers so that illumination directly charges the device; in integrated PV–SC packages, a solar cell is hard-wired to an EDLC or pseudocapacitor inside a single module. Reviews of integrated systems (including perovskites and dye cells) emphasize how spectrum, irradiance, and the operating point (direct coupling vs. MPP tracking) control round-trip efficiency and self-discharge—practical levers when you want “charge-under-light, power-in-the-dark” behavior [122]. A concrete monolithic example is the photo-rechargeable Zn-ion capacitor where 2D graphitic carbon nitride does double duty as light harvester and capacitor electrode, delivering direct light-driven charging under visible illumination [123]. When moving from sunlight to LED bench setups, the appeal is spectral selectivity and repeatability. Oxide and layered-carbon electrodes often

 doi:10.20944/preprints202511.0205.v1

show reproducible light-dependent gains that you can separate into photocapacitive (carrier-driven) and photothermal (temperature-driven) parts with simple controls. A representative case is V_2O_5 supercapacitors whose specific capacity increases under illumination; the study reports clear procedures—same geometry, calibrated irradiance—to isolate the optical contribution [124]. The broader photocapacitor literature recommends reporting irradiance at the device plane, spot size, duty cycle, and on/off transients alongside conventional Ragone and cycling data so results remain comparable across labs [121]. Laser stimulation during operation pushes this further because the beam can be tightly localized and modulated. Blue-diode excitation (≈450 nm) has been used to increase apparent charge-storage efficiency by injecting carriers and mildly warming the interface; the key is to publish fluence (mJ cm^{-2}), spot-averaged irradiance, and duty cycle to disentangle photocarrier and thermal routes [125]. The same lasers double as manufacturing tools: photonic-reduction stamping can pattern tens of thousands of graphene-based micro-supercapacitors in minutes, with pulse shaping and fluence dictating pore structure and sheet resistance—and therefore high-frequency response—after fabrication [126]. Figure 4 contrasts laser-patterned LIG/MnO_2 MSCs in three geometries—parallel strips, concentric rings, and interdigital—to illustrate how layout shapes rate handling and impedance. The side-by-side CV/GCD and impedance views underscore the benefit of designs that shorten ion paths and enlarge interfacial area for miniaturized MSCs [126].

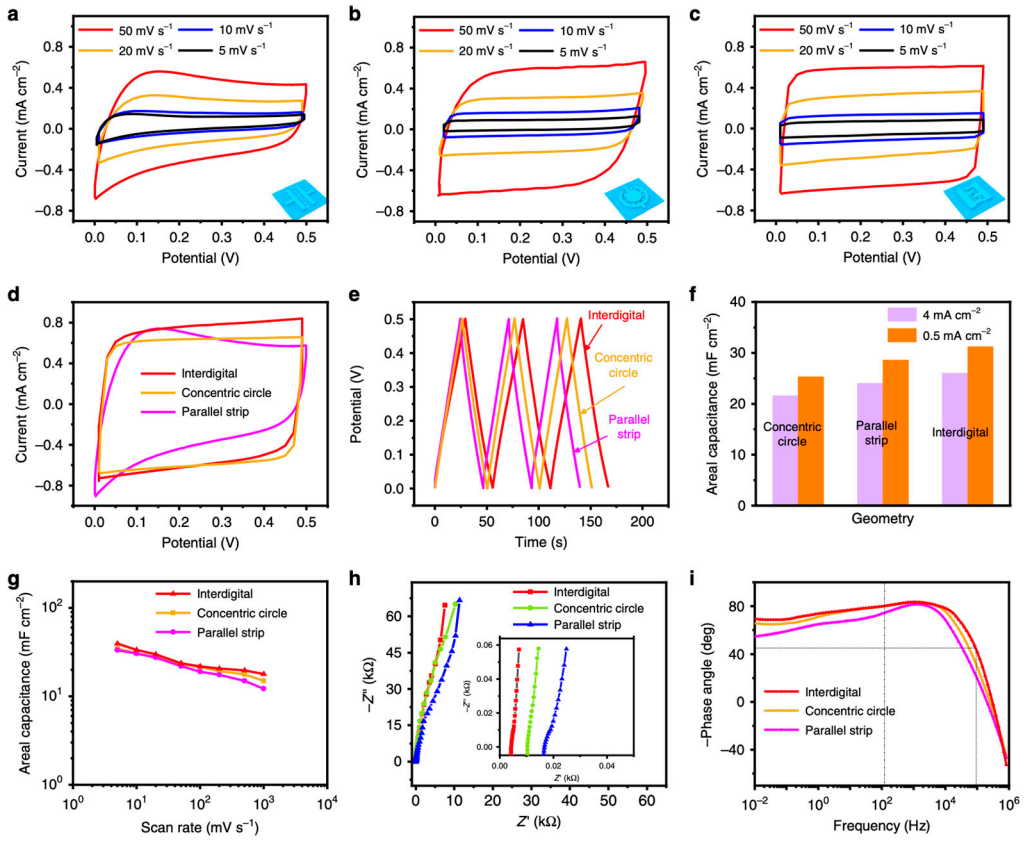

Figure 4. Electrochemical survey of laser-induced graphene/MnO_2 micro-supercapacitors (MSCs) built in several layouts. Cyclic voltammograms for parallel-strip, concentric-ring, and interdigital devices recorded in 0.5 M Na_2SO_4 over 100–1000 mV s^{-1} (a–c); CVs at 50 mV s^{-1} for a set of nonstandard MSC shapes in the same electrolyte (d); Galvanostatic charge–discharge traces obtained at 0.5 mA cm^{-2} (e); Areal capacitance for each geometry under low and high current loads (f); Capacitance as a function of scan rate for the three canonical layouts (g); Electrochemical impedance (Nyquist) spectra for the shape-varied MSCs (h); and Bode magnitude/phase plots highlighting frequency response across the designs (i). (Adapted with permission from ref. [126], Springer Nature 2020).

 doi:10.20944/preprints202511.0205.v1

The photothermal route has matured into a design strategy for cold-start or wide-temperature operation. By combining light-absorbing architectures with gel/ionogel electrolytes, groups routinely show stable capacitance across sub-zero to elevated temperatures; a recent example uses a gel polymer electrolyte to keep devices operable from −60 °C to 65 °C under light, explicitly quantifying the light-to-heat assist [127]. Materials engineering can also "bake in" solar absorption: MXene–wood composites boost light-to-heat conversion and, under sunlight, enhance energy storage in flexible cells [128]. Across these modalities, a few good-practice habits pay off. Calibrate irradiance at the device plane (thermopile or photodiode) and log surface temperature (IR camera or thermistor) so you can bound photothermal artifacts; use optical chopping or LED modulation with lock-in detection when signals are small; and, for integrated PV–SCs, compare "direct-coupled" vs. MPP-tracked operation so your reported gains reflect true photovoltaic-to-storage efficiency rather than fortuitous biasing [121,122].

In short, light can supply charge (photocharging), accelerate it (photothermal assistance), or even create the micro-architectures that make both efficient (laser processing). Choosing the route that matches your material and test envelope, and documenting the optical conditions with the same rigor used for electrochemistry, turns photonic stimulation from a lab curiosity into a reproducible design tool for next-generation supercapacitors.

6.4. Key Performance Parameters

For dual-function devices that store charge while sensing their environment and, in some cases, operate under illumination, the credibility of the results depends less on absolute numbers than on how the canonical metrics are defined and extracted. Four parameters frame most comparisons: the specific capacitance reported in the dark and under light; the energy and power densities derived from full-cell operation; the response time of the sensing function; and the cycling stability under electrochemical, mechanical, and optical stress. What follows adopts community conventions so that data from different laboratories and formats (bulk, flexible, and micro-supercapacitors) remain comparable.

Specific capacitance under dark and under illumination. Capacitance is most defensibly obtained from two-electrode galvanostatic discharge, taking the slope of the linear region and normalizing by mass, area, or volume according to form factor. This approach avoids the well-known inflation that can occur with three-electrode tests and should be treated as the primary figure of merit, with CV-derived values reported only as corroborative and explicitly scan-rate dependent [104]. When light is applied, optical conditions at the device plane—spectrum (e.g., AM1.5G), irradiance, spot size, duty cycle, and device temperature—ought to be stated alongside the pair (C_{dark}, C_{light}) A dimensionless photocapacitive gain $G=C_{light}/C_{dark}$ at fixed current density and temperature provides a compact summary and is now standard in photocapacitor work [121].

Energy and power density. Device-level energy is best computed by integrating the actual discharge curve, $E=\int I\,V(t)\,dt$, reserving $E=1/2C_{cell}V^2_{max}$ for strictly linear, hysteresis-free traces. Power follows as $P=E/\Delta t$, and results are ideally summarized in Ragone coordinates. Because constraints differ by scale, planar microsupercapacitors should report areal and volumetric figures side-by-side, whereas bulk/flexible cells typically emphasize gravimetric values; this dual reporting is now common practice for on-chip devices where footprint, not active mass, is limiting [129]. Where rate capability is central, quoting the rated-power estimate $P_{max}\approx V^2/(4\,ESR)$ derived from the IR drop is informative, but the headline power should remain the one obtained from the measured discharge [104]. Finally, interpretation of absolute capacitance should acknowledge the sensitivity of EDLCs to ion–pore matching, which can enhance or depress baseline performance independently of illumination or sensing [99].

Response time (sensing function). For humidity or gas sensing on the same platform, response and recovery are most transparently defined as the 10–90 % rise and 90–10 % decay of the chosen readout—capacitance, impedance, or resonance frequency—upon a step in analyte concentration, with the step amplitude and flow geometry explicitly described. Nanostructured oxide dielectrics

 doi:10.20944/preprints202511.0205.v1

(e.g., glancing-angle-deposited TiO_2) routinely reach sub-second dynamics, with thickness and porosity setting the characteristic times [90]. Graphene-family dielectrics such as graphene oxide achieve millisecond-to-second responses depending on film thickness and interrogation frequency [82]. When the sensor is frequency-encoded—for example, a graphene varactor coupled to an inductor—both the time constant and the sensitivity slope (e.g., kHz per %RH) should be reported; a widely cited implementation exhibits a linear ~5.7 kHz/%RH across 1–97 % RH at room temperature, with the mechanism traced to graphene's quantum capacitance [77,95].

Cycling stability. Stability is multidimensional and should be partitioned accordingly. Electrochemical cycling data benefit from plotting capacitance retention and coulombic efficiency versus cycle number under a fixed protocol (current density, voltage window, temperature), with the evolution of ESR reported in parallel because an increasing ESR is often the earliest indicator of degradation [104]. Calendar aging is captured by float tests (leakage current at a defined hold) and self-discharge curves (open-circuit voltage decay), ideally referenced to a recognized protocol to ease industrial comparison. For flexible and micro-scale formats, mechanical endurance (bending radius, strain state, number of bends) and, in light-coupled devices, illumination endurance (on/off cycles at stated irradiance and spectrum) complement the electrochemical picture; photocapacitor studies further recommend reporting photocharging efficiency alongside standard Ragone and cycling results [121].

Taken together, this framework treats the supercapacitor as a device. By extracting capacitance from two-electrode operation, normalizing energy and power on the basis most relevant to the intended form factor, defining sensing transients with clear kinetics, and disclosing stability across electrical, mechanical, and optical dimensions, the resulting metrics become portable across architectures and laboratories and thus suitable for a comparative review.

To contextualize the diversity of device formats surveyed, the Table 2 compiles representative systems that together span on-chip microsupercapacitors, flexible and fiber architectures, photo-assisted/storage-under-light devices, and truly capacitive sensing platforms.

Table 2. Representative TiO_2- and graphene-based capacitive sensors: materials, configuration, analyte, performance and mechanism.

Category	System / Materials	Architecture	Key metric(s)	Stability (headline)	Reference
On-chip MSC (carbon)	Onion-like carbon (OLC) interdigital MSC	Planar micro-interdigital on Si/Au	Vol. capacitance ≈ 1.3 F cm^{-3}; high-rate operation (up to ~200 V s^{-1})	≈10,000 cycles	[105]
On-chip MSC (CDC)	Monolithic carbide-derived carbon (from TiC)	Monolithic micro-MSC	High volumetric performance (paper benchmark)	Robust cycling	[106]
Flexible SC (graphene)	Laser-scribed graphene (LSG)	Planar thin-film on flexible substrate	Vol. power ≈ 200 W cm^{-3}; RC ≈ 19 ms	Stable under bending/twisting	[108]

 doi:10.20944/preprints202511.0205.v1

Capacitive sensor (graphene)	Graphene quantum-capacitance varactor (wireless)	Metal–oxide–graphene varactor + inductor (LC readout)	Sensitivity ≈ 5.7 ± 0.3 kHz/%RH (1–97% RH)	Passive wireless operation	[77]
Photo-rechargeable device	g-C_3N_4 photo-rechargeable Zn-ion capacitor	Sandwich Zn-ion capacitor; photoactive cathode	C ≈ 11.377 F g^{-1}; photo-charging ΔV ≈ 0.85 V (AM1.5G)	≈90% capacitance retention over 1000 cycles	[123]

7. Challenges and Future Perspectives

Bringing storage, sensing, and—in some cases—light responsiveness into a single supercapacitor has moved from aspiration to proof-of-concept. What now stands between laboratory elegance and field-ready systems is less a single "missing material" than a set of intertwined constraints: how signals are generated, where they travel, and how they drift over time.

At the heart of every dual-function device lies cross-talk. The same porosity that delivers large double-layer capacitance also admits water and gases, changing permittivity and interfacial polarization. In practice, the device never shows a single capacitance but a spectrum that shifts with frequency, bias history, and ambient conditions. The most successful prototypes already treat this not as noise but as a resource: a high-frequency window for sensing, a low-frequency window for storage, and carefully chosen biases that maximize sensitivity without eroding the electrolyte's stability. As this mindset spreads, it should become routine to "listen" in one band while "working" in another.

Selectivity remains the quiet challenge. Capacitive transduction is wonderfully low-power, yet unashamedly catholic in what it responds to—humidity, temperature, co-adsorbed gases, gentle mechanical strain. Chemistry helps (tailored surface groups on oxides, defect engineering in GO, or quantum-capacitance readout in graphene), but architecture matters just as much. Differential layouts—an active lane beside a reference lane, both interrogated at two or more frequencies—can allow subtraction in hardware rather than in wishful thinking. The field is likely to converge on such "paired" designs because they scale well, both in arrays and in time. Long-term stability is less glamorous than peak sensitivity, yet it is what turns a figure in a paper into a device someone can trust. Oxide dielectrics need surfaces that can be cleaned or reset without heaters; layered carbons need to swell without ungluing; graphene varactors need buried interfaces that do not wick in water for months. Small, scheduled acts of maintenance—brief UV refresh for photocatalytic oxides, short conditioning pulses for GO, occasional reference sweeps at a diagnostic frequency—are becoming part of the operating rhythm rather than afterthoughts. Light will keep playing three roles at once. It can add charge directly (photocharging), accelerate it (photothermal assistance), and even carve the very micro-architectures that make both efficient (laser writing and reduction). The opportunity now is not to discover yet another illumination effect, but to make the existing ones portable across laboratories: quote irradiance at the device plane, log surface temperature, modulate the beam, and report a small set of photo-metrics (gain under light, photo-charging efficiency, on/off endurance). With these habits, optical knobs become design parameters instead of confounding factors.

On the electrolyte front, the community is beginning to accept that one formulation must serve two masters. Wide windows and high conductivity are essential for energy, but they can also mask or distort sensing. Conversely, gels that beautifully track ambient humidity may tempt the sensor while undermining storage. The path forward looks like deliberate compromise: electrolytes and interphases that are chemically dull where they should be (stable, non-reactive) and exquisitely tuned at the sensing interface. "Water-in-salt" chemistries, ionogels, and hybrid solid–liquid systems are all being recruited to that end.

 doi:10.20944/preprints202511.0205.v1

Manufacturability is no longer an afterthought. Laser-scribed graphene, printed MXene and carbon inks, and wafer-level microsupercapacitors have shown that it is possible to go from sketch to sheet or chip in a day. The next barrier is mundane and decisive: interconnect resistance in large arrays, ink uniformity over meters, and encapsulation that breathes for sensing but seals for storage. Expect more attention to current-collector meshes, diffusion windows, and edge-sealed ionogels, the quiet plumbing that makes headline metrics repeatable.

Finally, as devices become multifunctional, honest benchmarking becomes a public good. A short, journal-neutral checklist goes a long way: report two-electrode capacitance from galvanostatic discharge; place energy and power on the basis that matches the form factor (gravimetric for bulk, areal/volumetric for micros); define sensing transients with 10–90% kinetics and step amplitudes; disclose light conditions and device temperature; track ESR, float behavior, and self-discharge. Where possible, share raw traces. The payoff is immediate: apples-to-apples plots, reproducible meta-analyses, and faster iteration.

Looking ahead, progress will be systems-level. Mechanism-aware readout (frequency and bias multiplexing) will let a cell store and sense without tripping over itself. Interfaces—those nanometers of oxide, carbon, gel, and trapped water—will receive the meticulous engineering once reserved for bulk materials. Photonic coupling will be treated as matched impedance rather than an add-on. And print-and-laser workflows will merge with roll-to-roll encapsulation and textile integration, turning one-off demonstrators into panels and garments that survive weather, washing, and weeks of unattended operation. In that future, the most interesting supercapacitors will be the ones that are barely noticed: quiet, thin, and relentless, storing energy while telling us—reliably—what the environment is doing.

8. Conclusions

This review has traced how supercapacitors can be engineered to store charge while sensing their environment—and, in many cases, to respond productively to light. Across materials and formats, three insights stand out. First, capacitive sensing in oxides and graphene-family films is governed by a small set of physical channels—dielectric/interfacial polarization, EDL/ion transport, and, for graphene, quantum capacitance—that can be intentionally separated in frequency and bias. Second, form follows function: hierarchical porosity and thin, tortuous films let devices reconcile large double-layer storage with fast analyte access, while differential layouts and frequency-encoded readout improve selectivity at room temperature. Third, credible benchmarking hinges on device-level metrology: two-electrode capacitance from galvanostatic discharge, Ragone plots normalized to the relevant basis (gravimetric for bulk; areal/volumetric for micros), 10–90% sensing transients with explicit step amplitudes, and stability that spans electrochemical, mechanical, and illumination endurance. With these practices, reported gains in capacitance, energy, or sensing can be meaningfully compared across laboratories and architectures. A consistent performance trend emerges from the literature. TiO_2, especially in nanocolumnar or mesoporous morphologies, delivers large, frequency-dispersive dielectric responses for humidity sensing at room temperature and can be photocatalytically regenerated to suppress drift. Graphene and graphene oxide add complementary levers: GO's water uptake and permittivity swing furnish strong capacitive signals in planar IDE formats, while graphene varactors exploit quantum capacitance to translate adsorbate-induced Fermi-level shifts into precise changes in C or resonant frequency, enabling wireless, μW-level readout. At the system level, frequency/bias multiplexing allows the same footprint to be interrogated in a "sensing band" without disturbing charge storage in its "power band," and photo-assistance (solar/LED/laser) can either supply charge directly (photocharging) or reduce ESR via controlled photothermal heating—provided temperature and irradiance are rigorously disclosed. Within this landscape, photoresponsive TiO_2/graphene hybrids stand out as a practical platform for multifunctional, next-generation energy devices. The pairing is naturally synergistic: TiO_2 provides a robust, regenerable dielectric interface with strong UV responsivity, while graphene (or GO) contributes high conductivity, tunable surface chemistry, and, uniquely, quantum-capacitance

 doi:10.20944/preprints202511.0205.v1

transduction. Architectures that place graphene or GO atop photoactive TiO_2 (or interleave them in layered stacks) can therefore (i) store energy with EDLC-class kinetics, (ii) sense humidity or selected gases via dielectric or quantum-capacitance pathways, and (iii) harness light to reset surfaces, accelerate kinetics, or even photo-recharge under standard irradiance. Such hybrids map cleanly onto flexible and microscale formats—laser/printed graphene, GLAD/sol–gel TiO_2—and are compatible with solid or gel electrolytes, paving a realistic path to skin- and chip-integrated power-sensing modules. Realizing that promise will depend on interdisciplinary efforts. Materials chemists are needed to stabilize buried interfaces and tailor surface groups for selectivity without drift. Device physicists and electrochemists must formalize frequency/bias partitioning so storage and sensing operate without cross-talk. Photonics and thermal experts can standardize optical coupling and decouple photocarrier from photothermal effects. Manufacturing scientists will translate one-off demonstrators into arrays through printable inks, laser patterning, low-ESR interconnects, and breathable-yet-hermetic encapsulation. Finally, metrology and data-science communities can cement honest, portable benchmarking and curate open datasets that accelerate design loops (e.g., ion–pore matching, differential sensor layouts, and lifetime models).

As summary, the building blocks are in place: porous TiO_2 for strong, regenerable dielectric transduction; graphene-family materials for high-rate storage and quantum-capacitance sensing; and photonic stimulation as a controllable auxiliary. The near-term advances will be systems-level—interfaces, packaging, protocols—turning elegant prototypes into reliable, unobtrusive devices that store energy while measuring the world in real time.

Supplementary Materials: The following supporting information can be downloaded at the website of this paper posted on Preprints.org.

Author Contributions: Conceptualization, F.M.; methodology, F.M.; formal analysis, M.C., J.D., F.D., C.M., and F.M.; investigation, M.C., J.D., F.D., I.G., C.N., C.M., and F.M.; resources, C.M., F.M.; writing—original draft preparation, F.M.; writing—review and editing, M.C., J.D., F.D., C.M., and F.M.; supervision, F.M.; project administration, F.M.; funding acquisition, M.C., J.D., F.D., C.M., and F.M. All authors have read and agreed to the published version of the manuscript.

Funding: The authors gratefully acknowledge financial support from the NSF Center for the Advancement of Wearable Technologies (CAWT, Grant 1849243), the Consortium of Hybrid Resilient Energy Systems (CHRES, Grant DE-NA0003982). This work was also supported by the Spanish Ministry of Science, Innovation and Universities and the State Research Agency (MICIU/AEI) within the framework of the EU M-ERA.NET Program (SOLIMEC project, Spanish subproject PCI2022-132998).

Institutional Review Board Statement: Not applicable.

Informed Consent Statement: Not applicable.

Data Availability Statement: The data is contained in the article and is available from the authors on reasonable request.

Acknowledgments: The authors gratefully acknowledge Raúl S. García, Dock García and Dina Márquez, for their valuable assistance in organizing and updating the research databases, as well as for their support in coordinating the bibliography.

Conflicts of Interest: The authors declare no conflict of interest.

Abbreviations

The following abbreviations are used in this manuscript:

ALD	Atomic Layer Deposition
AM1.5G	Air Mass 1.5 Global (solar irradiance standard)
CDC	Carbide-Derived Carbon

 doi:10.20944/preprints202511.0205.v1

CNT(s)	Carbon Nanotube(s)
CVD	Chemical Vapor Deposition
DOS	Density of States
EDL	Electric Double Layer
EDLC(s)	Electric Double-Layer Capacitor(s)
EIS	Electrochemical Impedance Spectroscopy
ESR	Equivalent Series Resistance
g-C_3N_4	Graphitic Carbon Nitride
GLAD	Glancing-Angle Deposition
GO	Graphene Oxide
HfO_2	Hafnium(IV) Oxide
H_2O	Water
IDE(s)	Interdigitated Electrode(s)
IoT	Internet of Things
LC	Inductor–Capacitor (wireless resonant readout)
LSG	Laser-Scribed Graphene
LSPR	Localized Surface Plasmon Resonance
MWS	Maxwell–Wagner–Sillars (interfacial polarization)
MXene(s)	2D Transition-Metal Carbides/Nitrides (e.g., $Ti_3C_2T_x$)
NH_3	Ammonia
NO_2	Nitrogen Dioxide
OLC	Onion-Like Carbon
PV	Photovoltaic
PVA	Poly(vinyl alcohol) (gel electrolyte)
rGO	Reduced Graphene Oxide
RH	Relative Humidity
SC	Supercapacitor
TiO_2	Titanium Dioxide
UV	Ultraviolet
VOC(s)	Volatile Organic Compound(s)
WIS	Water-in-Salt (electrolyte)

References

1. Simon, P.; Gogotsi, Y. Materials for Electrochemical Capacitors. *Nature Mater* **2008**, *7*, 845–854, doi:10.1038/nmat2297.
2. Tarascon, J.-M.; Armand, M. Issues and Challenges Facing Rechargeable Lithium Batteries. *Nature* **2001**, *414*, 359–367, doi:10.1038/35104644.
3. Conway, B. E. *Electrochemical Supercapacitors*; Springer, 1999;
4. Béguin, F.; Frackowiak, E. *Supercapacitors: Materials, Systems and Applications*; Wiley-VCH, 2013;
5. Wang, G.; Zhang, L.; Zhang, J. A Review of Electrode Materials for Electrochemical Supercapacitors. *Chem. Soc. Rev.* **2012**, *41*, 797–828, doi:10.1039/C1CS15060J.
6. Low, J.; Yu, J.; Jaroniec, M.; Wageh, S.; Al-Ghamdi, A.A. Heterojunction Photocatalysts. *Advanced Materials* **2017**, *29*, 1601694, doi:10.1002/adma.201601694.

 doi:10.20944/preprints202511.0205.v1

7. Diebold, U. The Surface Science of Titanium Dioxide. *Surface Science Reports* **2003**, *48*, 53–229, doi:10.1016/S0167-5729(02)00100-0.
8. O'Regan, B.; Grätzel, M. A Low-Cost, High-Efficiency Solar Cell Based on Dye-Sensitized Colloidal TiO2 Films. *Nature* **1991**, *353*, 737–740, doi:10.1038/353737a0.
9. Fujishima, A.; Honda, K. Electrochemical Photolysis of Water at a Semiconductor Electrode. *Nature* **1972**, *238*, 37–38, doi:10.1038/238037a0.
10. Novoselov, K.S.; Geim, A.K.; Morozov, S.V.; Jiang, D.; Zhang, Y.; Dubonos, S.V.; Grigorieva, I.V.; Firsov, A.A. Electric Field Effect in Atomically Thin Carbon Films. *Science* **2004**, *306*, 666–669, doi:10.1126/science.1102896.
11. Ke, Q.; Wang, J. Graphene-Based Materials for Supercapacitor Electrodes – A Review. *Journal of Materiomics* **2016**, *2*, 37–54, doi:10.1016/j.jmat.2016.01.001.
12. Volfkovich, Y.M.; Rychagov, A.Y.; Sosenkin, V.E.; Baskakov, S.A.; Kabachkov, E.N.; Shulga, Y.M. Supercapacitor Properties of rGO-TiO2 Nanocomposite in Two-Component Acidic Electrolyte. *Materials* **2022**, *15*, 7856, doi:10.3390/ma15217856.
13. Mannoor, M.S.; Tao, H.; Clayton, J.D.; Sengupta, A.; Kaplan, D.L.; Naik, R.R.; Verma, N.; Omenetto, F.G.; McAlpine, M.C. Graphene-Based Wireless Bacteria Detection on Tooth Enamel. *Nat Commun* **2012**, *3*, 763, doi:10.1038/ncomms1767.
14. Omidvar, A.; Mohajeri, A. Edge-Functionalized Graphene Nanoflakes as Selective Gas Sensors. *Sensors and Actuators B: Chemical* **2014**, *202*, 622–630, doi:10.1016/j.snb.2014.05.136.
15. Zhu, Y.; Murali, S.; Cai, W.; Li, X.; Suk, J.W.; Potts, J.R.; Ruoff, R.S. Graphene and Graphene Oxide: Synthesis, Properties, and Applications. *Advanced Materials* **2010**, *22*, 3906–3924, doi:10.1002/adma.201001068.
16. Conway, B.E.; Birss, V.; Wojtowicz, J. The Role and Utilization of Pseudocapacitance for Energy Storage by Supercapacitors. *Journal of Power Sources* **1997**, *66*, 1–14, doi:10.1016/S0378-7753(96)02474-3.
17. Wei, Y.-M.; Kumar, K.D.; Zhang, L.; Li, J.-F. Pseudocapacitive Materials for Energy Storage: Properties, Mechanisms, and Applications in Supercapacitors and Batteries. *Front. Chem.* **2025**, *13*, 1636683, doi:10.3389/fchem.2025.1636683.
18. Lakshmi, K.C.S.; Vedhanarayanan, B. High-Performance Supercapacitors: A Comprehensive Review on Paradigm Shift of Conventional Energy Storage Devices. *Batteries* **2023**, *9*, 202, doi:10.3390/batteries9040202.
19. Lim, J.M.; Jang, Y.S.; Van T. Nguyen, H.; Kim, J.S.; Yoon, Y.; Park, B.J.; Seo, D.H.; Lee, K.-K.; Han, Z.; Ostrikov, K. (Ken); et al. Advances in High-Voltage Supercapacitors for Energy Storage Systems: Materials and Electrolyte Tailoring to Implementation. *Nanoscale Adv.* **2023**, *5*, 615–626, doi:10.1039/D2NA00863G.
20. Al-Hamry, A.; Pašti, I.A.; Kanoun, O. Titanium Dioxide/Graphene Oxide Nanocomposite-Based Humidity Sensors with Improved Performance. *J. Compos. Sci.* **2025**, *9*, 60, doi:10.3390/jcs9020060.
21. Chen, X.; Mao, S.S. Titanium Dioxide Nanomaterials: Synthesis, Properties, Modifications, and Applications. *Chem. Rev.* **2007**, *107*, 2891–2959, doi:10.1021/cr0500535.
22. Wang, G.; Ling, Y.; Li, Y. Oxygen-Deficient Metal Oxide Nanostructures for Photoelectrochemical Water Oxidation and Other Applications. *Nanoscale* **2012**, *4*, 6682, doi:10.1039/c2nr32222f.
23. Wang, G.; Wang, H.; Ling, Y.; Tang, Y.; Yang, X.; Fitzmorris, R.C.; Wang, C.; Zhang, J.Z.; Li, Y. Hydrogen-Treated TiO_2 Nanowire Arrays for Photoelectrochemical Water Splitting. *Nano Lett.* **2011**, *11*, 3026–3033, doi:10.1021/nl201766h.
24. Wu, W.; Peng, Z.; Wang, J.; Li, X.; Deng, P.; Zhou, Y.; Jia, G.; Ye, W.; Gao, P. Surface Oxygen Vacancy Engineering on TiO_2 (101) *via* ALD Technology for Simultaneously Enhancing Charge Separation and Transfer. *Chem. Commun.* **2023**, *59*, 3237–3240, doi:10.1039/D2CC06853B.
25. Altaf, C.T.; Coskun, O.; Kumtepe, A.; Rostas, A.M.; Iatsunskyi, I.; Coy, E.; Erdem, E.; Sankir, M.; Sankir, N.D. Photo-Supercapacitors Based on Nanoscaled ZnO. *Sci Rep* **2022**, *12*, 11487, doi:10.1038/s41598-022-15180-z.
26. Flores-Diaz, N.; De Rossi, F.; Keller, T.; Morritt, H.; Perez Bassart, Z.; Lopez-Rubio, A.; Jose Fabra, M.; Freitag, R.; Gagliardi, A.; Fasulo, F.; et al. Unlocking High-Performance Photocapacitors for Edge Computing in Low-Light Environments. *Energy Environ. Sci.* **2025**, *18*, 4704–4716, doi:10.1039/D5EE01052G.

27. Azadmanjiri, J.; Sturala, J.; Regner, J.; Oliveira, F.M.; Mazánek, V.; Sofer, Z. Tuning Germanane Band Gaps via Cyanoethyl Functionalization for Cutting-Edge Photoactive Cathodes: Photoenhanced Hybrid Zinc-Ion Capacitor Evaluation. *ACS Appl. Mater. Interfaces* **2024**, *16*, 14722–14741, doi:10.1021/acsami.3c17420.
28. Kumar, S.; Mondal, A.; Panwar, V.; Shekhawat, R.; Misra, A. Highly Efficient Photo Rechargeable Supercapacitor Based on Ambipolar Interface of Graphitic Carbon Nitride and MXene. *Batteries & Supercaps* **2024**, *7*, e202300393, doi:10.1002/batt.202300393.
29. Su, Y.-S.; Fu, Y.; Cochell, T.; Manthiram, A. A Strategic Approach to Recharging Lithium-Sulphur Batteries for Long Cycle Life. *Nat Commun* **2013**, *4*, 2985, doi:10.1038/ncomms3985.
30. Plebankiewicz, I.; Bogdanowicz, K.A.; Iwan, A. Photo-Rechargeable Electric Energy Storage Systems Based on Silicon Solar Cells and Supercapacitor-Engineering Concept. *Energies* **2020**, *13*, 3867, doi:10.3390/en13153867.
31. Ohtani, B. Photocatalysis A to Z—What We Know and What We Do Not Know in a Scientific Sense. *Journal of Photochemistry and Photobiology C: Photochemistry Reviews* **2010**, *11*, 157–178, doi:10.1016/j.jphotochemrev.2011.02.001.
32. Chen, X.; Liu, L.; Huang, F. Black Titanium Dioxide (TiO_2) Nanomaterials. *Chem. Soc. Rev.* **2015**, *44*, 1861–1885, doi:10.1039/C4CS00330F.
33. Wu, H.B.; Xia, B.Y.; Yu, L.; Yu, X.-Y.; Lou, X.W. Porous Molybdenum Carbide Nano-Octahedrons Synthesized via Confined Carburization in Metal-Organic Frameworks for Efficient Hydrogen Production. *Nat Commun* **2015**, *6*, 6512, doi:10.1038/ncomms7512.
34. Jiang, C.; Moniz, S.J.A.; Wang, A.; Zhang, T.; Tang, J. Photoelectrochemical Devices for Solar Water Splitting – Materials and Challenges. *Chem. Soc. Rev.* **2017**, *46*, 4645–4660, doi:10.1039/C6CS00306K.
35. Roy, P.; Berger, S.; Schmuki, P. TiO_2 Nanotubes: Synthesis and Applications. *Angew Chem Int Ed* **2011**, *50*, 2904–2939, doi:10.1002/anie.201001374.
36. Asahi, R.; Morikawa, T.; Ohwaki, T.; Aoki, K.; Taga, Y. Visible-Light Photocatalysis in Nitrogen-Doped Titanium Oxides. *Science* **2001**, *293*, 269–271, doi:10.1126/science.1061051.
37. Choi, W.; Termin, A.; Hoffmann, M.R. The Role of Metal Ion Dopants in Quantum-Sized TiO_2 : Correlation between Photoreactivity and Charge Carrier Recombination Dynamics. *J. Phys. Chem.* **1994**, *98*, 13669–13679, doi:10.1021/j100102a038.
38. Khan, S.U.M.; Al-Shahry, M.; Ingler, W.B. Efficient Photochemical Water Splitting by a Chemically Modified N-TiO_2. *Science* **2002**, *297*, 2243–2245, doi:10.1126/science.1075035.
39. Livage, J.; Henry, M.; Sanchez, C. Sol-Gel Chemistry of Transition Metal Oxides. *Progress in Solid State Chemistry* **1988**, *18*, 259–341, doi:10.1016/0079-6786(88)90005-2.
40. Zhou, W.; Li, W.; Wang, J.-Q.; Qu, Y.; Yang, Y.; Xie, Y.; Zhang, K.; Wang, L.; Fu, H.; Zhao, D. Ordered Mesoporous Black TiO_2 as Highly Efficient Hydrogen Evolution Photocatalyst. *J. Am. Chem. Soc.* **2014**, *136*, 9280–9283, doi:10.1021/ja504802q.
41. Bastug Azer, B.; Gulsaran, A.; Pennings, J.R.; Karimi, R.; Ashrafi Belgabad, A.; Xu, A.H.; Zaidan, L.; Kocer, S.; Sanderson, J.; Bajcsy, M.; et al. Core–Shell Defective TiO_2 Nanoparticles by Femtosecond Laser Irradiation with Enhanced Photocatalytic Performance. *Mater. Adv.* **2023**, *4*, 1297–1305, doi:10.1039/D3MA00019B.
42. Amendola, V.; Amans, D.; Ishikawa, Y.; Koshizaki, N.; Scirè, S.; Compagnini, G.; Reichenberger, S.; Barcikowski, S. Room-Temperature Laser Synthesis in Liquid of Oxide, Metal-Oxide Core-Shells, and Doped Oxide Nanoparticles. *Chemistry A European J* **2020**, *26*, 9206–9242, doi:10.1002/chem.202000686.
43. Meierhofer, F.; Fritsching, U. Synthesis of Metal Oxide Nanoparticles in Flame Sprays: Review on Process Technology, Modeling, and Diagnostics. *Energy Fuels* **2021**, *35*, 5495–5537, doi:10.1021/acs.energyfuels.0c04054.
44. Trovarelli, A.; Llorca, J. Ceria Catalysts at Nanoscale: How Do Crystal Shapes Shape Catalysis? *ACS Catal.* **2017**, *7*, 4716–4735, doi:10.1021/acscatal.7b01246.
45. Puurunen, R.L. Surface Chemistry of Atomic Layer Deposition: A Case Study for the Trimethylaluminum/Water Process. *Journal of Applied Physics* **2005**, *97*, 121301, doi:10.1063/1.1940727.
46. Wang, B.; Ruan, T.; Chen, Y.; Jin, F.; Peng, L.; Zhou, Y.; Wang, D.; Dou, S. Graphene-Based Composites for Electrochemical Energy Storage. *Energy Storage Materials* **2020**, *24*, 22–51, doi:10.1016/j.ensm.2019.08.004.

47. *Carbon Nanotubes*; Dresselhaus, M.S., Dresselhaus, G., Avouris, P., Eds.; Topics in Applied Physics; Springer Berlin Heidelberg: Berlin, Heidelberg, 2001; Vol. 80; ISBN 978-3-540-41086-7.
48. Cheng, P.; Yang, Z.; Wang, H.; Cheng, W.; Chen, M.; Shangguan, W.; Ding, G. TiO2–Graphene Nanocomposites for Photocatalytic Hydrogen Production from Splitting Water. *International Journal of Hydrogen Energy* **2012**, *37*, 2224–2230, doi:10.1016/j.ijhydene.2011.11.004.
49. Fan, W.; Lai, Q.; Zhang, Q.; Wang, Y. Nanocomposites of TiO_2 and Reduced Graphene Oxide as Efficient Photocatalysts for Hydrogen Evolution. *J. Phys. Chem. C* **2011**, *115*, 10694–10701, doi:10.1021/jp2008804.
50. S., J.B.; Muniyappa, M.; V., N.R.; Mudike, R.; Shastri, M.; Tathagata, S.; Shivaramu, P.D.; M.V., S.; C.S., A.K.; Rangappa, D. Enhanced Photocatalytic Hydrogen Evolution from Reduced Graphene Oxide-Defect Rich TiO2-x Nanocomposites. *International Journal of Hydrogen Energy* **2022**, *47*, 40242–40253, doi:10.1016/j.ijhydene.2022.07.115.
51. Poirot, N.; Rajalingam, V.; Murgu, R.N.; Omnée, R.; Raymundo-Piñero, E. Nanotexturing TiO2 over Carbon Nanotubes for High-Energy and High-Power Density Pseudocapacitors in Organic Electrolytes. *Front. Mater.* **2022**, *9*, 1011782, doi:10.3389/fmats.2022.1011782.
52. Yadav, P.; Pandey, K.; Bhatt, P.; Tripathi, B.; Pandey, M.K.; Kumar, M. Probing the Electrochemical Properties of TiO2/Graphene Composite by Cyclic Voltammetry and Impedance Spectroscopy. *Materials Science and Engineering: B* **2016**, *206*, 22–29, doi:10.1016/j.mseb.2015.12.007.
53. Li, Z.; Liu, Z.; Yang, X.; Chen, A.; Chen, P.; Yang, L.; Yan, C.; Shi, Y. Enhanced Photocatalysis of Black TiO2/Graphene Composites Synthesized by a Facile Sol–Gel Method Combined with Hydrogenation Process. *Materials* **2022**, *15*, 3336, doi:10.3390/ma15093336.
54. Giampiccolo, A.; Tobaldi, D.M.; Leonardi, S.G.; Murdoch, B.J.; Seabra, M.P.; Ansell, M.P.; Neri, G.; Ball, R.J. Sol Gel Graphene/TiO2 Nanoparticles for the Photocatalytic-Assisted Sensing and Abatement of NO2. *Applied Catalysis B: Environmental* **2019**, *243*, 183–194, doi:10.1016/j.apcatb.2018.10.032.
55. Nongthombam, S.; Swain, B.P. Hydrothermal Synthesis of rGO-TiO2 Nanocomposites for Electrochemical Performance. *J Appl Electrochem* **2024**, *54*, 809–821, doi:10.1007/s10800-023-01998-6.
56. Ruidíaz-Martínez, M.; Álvarez, M.A.; López-Ramón, M.V.; Cruz-Quesada, G.; Rivera-Utrilla, J.; Sánchez-Polo, M. Hydrothermal Synthesis of rGO-TiO2 Composites as High-Performance UV Photocatalysts for Ethylparaben Degradation. *Catalysts* **2020**, *10*, 520, doi:10.3390/catal10050520.
57. Zhang, H.; Lv, X.; Li, Y.; Wang, Y.; Li, J. P25-Graphene Composite as a High Performance Photocatalyst. *ACS Nano* **2010**, *4*, 380–386, doi:10.1021/nn901221k.
58. Endrődi, B.; Kecsenovity, E.; Rajeshwar, K.; Janáky, C. One-Step Electrodeposition of Nanocrystalline TiO_2 Films with Enhanced Photoelectrochemical Performance and Charge Storage. *ACS Appl. Energy Mater.* **2018**, *1*, 851–858, doi:10.1021/acsaem.7b00289.
59. Ban, C.; Xie, M.; Sun, X.; Travis, J.J.; Wang, G.; Sun, H.; Dillon, A.C.; Lian, J.; George, S.M. Atomic Layer Deposition of Amorphous TiO_2 on Graphene as an Anode for Li-Ion Batteries. *Nanotechnology* **2013**, *24*, 424002, doi:10.1088/0957-4484/24/42/424002.
60. Zhang, Y.; Guerra-Nuñez, C.; Utke, I.; Michler, J.; Agrawal, P.; Rossell, M.D.; Erni, R. Atomic Layer Deposition of Titanium Oxide on Single-Layer Graphene: An Atomic-Scale Study toward Understanding Nucleation and Growth. *Chem. Mater.* **2017**, *29*, 2232–2238, doi:10.1021/acs.chemmater.6b05143.
61. Sun, X.; Xie, M.; Travis, J.J.; Wang, G.; Sun, H.; Lian, J.; George, S.M. Pseudocapacitance of Amorphous TiO_2 Thin Films Anchored to Graphene and Carbon Nanotubes Using Atomic Layer Deposition. *J. Phys. Chem. C* **2013**, *117*, 22497–22508, doi:10.1021/jp4066955.
62. Nasir, A.; Khalid, S.; Yasin, T.; Mazare, A. A Review on the Progress and Future of TiO2/Graphene Photocatalysts. *Energies* **2022**, *15*, 6248, doi:10.3390/en15176248.
63. Zhang, H.; Shuang, S.; Wang, G.; Guo, Y.; Tong, X.; Yang, P.; Chen, A.; Dong, C.; Qin, Y. TiO_2 –Graphene Hybrid Nanostructures by Atomic Layer Deposition with Enhanced Electrochemical Performance for Pb(II) and Cd(II) Detection. *RSC Adv.* **2015**, *5*, 4343–4349, doi:10.1039/C4RA09779C.
64. Xiang, C.; Li, M.; Zhi, M.; Manivannan, A.; Wu, N. Reduced Graphene Oxide/Titanium Dioxide Composites for Supercapacitor Electrodes: Shape and Coupling Effects. *J. Mater. Chem.* **2012**, *22*, 19161, doi:10.1039/c2jm33177b.

 doi:10.20944/preprints202511.0205.v1

65. Ramadoss, A.; Kim, G.-S.; Kim, S.J. Fabrication of Reduced Graphene Oxide/TiO2 Nanorod/Reduced Graphene Oxide Hybrid Nanostructures as Electrode Materials for Supercapacitor Applications. *CrystEngComm* **2013**, *15*, 10222, doi:10.1039/c3ce41517a.
66. Kim, J.; Khoh, W.-H.; Wee, B.-H.; Hong, J.-D. Fabrication of Flexible Reduced Graphene Oxide–TiO_2 Freestanding Films for Supercapacitor Application. *RSC Adv.* **2015**, *5*, 9904–9911, doi:10.1039/C4RA12980F.
67. Jiang, L.; Ren, Z.; Chen, S.; Zhang, Q.; Lu, X.; Zhang, H.; Wan, G. Bio-Derived Three-Dimensional Hierarchical Carbon-Graphene-TiO2 as Electrode for Supercapacitors. *Sci Rep* **2018**, *8*, 4412, doi:10.1038/s41598-018-22742-7.
68. Lau, S.C.; Lim, H.N.; Ravoof, T.B.S.A.; Yaacob, M.H.; Grant, D.M.; MacKenzie, R.C.I.; Harrison, I.; Huang, N.M. A Three-Electrode Integrated Photo-Supercapacitor Utilizing Graphene-Based Intermediate Bifunctional Electrode. *Electrochimica Acta* **2017**, *238*, 178–184, doi:10.1016/j.electacta.2017.04.003.
69. Sankapal, B.R.; Gajare, H.B.; Dubal, D.P.; Gore, R.B.; Salunkhe, R.R.; Ahn, H. Presenting Highest Supercapacitance for TiO2/MWNTs Nanocomposites: Novel Method. *Chemical Engineering Journal* **2014**, *247*, 103–110, doi:10.1016/j.cej.2014.02.092.
70. Chen, Z.; Lu, C. Humidity Sensors: A Review of Materials and Mechanisms. *Sen Lett* **2005**, *3*, 274–295, doi:10.1166/sl.2005.045.
71. Anasori, B.; Lukatskaya, M.R.; Gogotsi, Y. 2D Metal Carbides and Nitrides (MXenes) for Energy Storage. *Nat Rev Mater* **2017**, *2*, 16098, doi:10.1038/natrevmats.2016.98.
72. Tang, X.; Debliquy, M.; Lahem, D.; Yan, Y.; Raskin, J.-P. A Review on Functionalized Graphene Sensors for Detection of Ammonia. *Sensors* **2021**, *21*, 1443, doi:10.3390/s21041443.
73. Maier, C.; Egger, L.; Köck, A.; Reichmann, K. A Review of Gas Sensors for CO2 Based on Copper Oxides and Their Derivatives. *Sensors* **2024**, *24*, 5469, doi:10.3390/s24175469.
74. Šetka, M.; Claros, M.; Chmela, O.; Vallejos, S. Photoactivated Materials and Sensors for NO_2 Monitoring. *J. Mater. Chem. C* **2021**, *9*, 16804–16827, doi:10.1039/D1TC04247E.
75. Steele, J.J.; Fitzpatrick, G.A.; Brett, M.J. Capacitive Humidity Sensors With High Sensitivity and Subsecond Response Times. *IEEE Sensors J.* **2007**, *7*, 955–956, doi:10.1109/JSEN.2007.897363.
76. Feng, J.; Kang, X.; Zuo, Q.; Yuan, C.; Wang, W.; Zhao, Y.; Zhu, L.; Lu, H.; Chen, J. Fabrication and Evaluation of a Graphene Oxide-Based Capacitive Humidity Sensor. *Sensors* **2016**, *16*, 314, doi:10.3390/s16030314.
77. Deen, D.A.; Olson, E.J.; Ebrish, M.A.; Koester, S.J. Graphene-Based Quantum Capacitance Wireless Vapor Sensors. *IEEE Sensors J.* **2014**, *14*, 1459–1466, doi:10.1109/JSEN.2013.2295302.
78. Ju, W.; Lee, S. Capacitive NO2 Detection Using CVD Graphene-Based Device. *Nanomaterials* **2023**, *13*, 243, doi:10.3390/nano13020243.
79. Bearzotti, A.; Bianco, A.; Montesperelli, G.; Traversa, E. Humidity Sensitivity of Sputtered TiO2 Thin Films. *Sensors and Actuators B: Chemical* **1994**, *19*, 525–528, doi:10.1016/0925-4005(93)01072-C.
80. Mohamed Zahidi, M.; Mamat, M.H.; Malek, M.F.; Yaakob, M.K.; Ahmad, M.K.; Abu Bakar, S.; Mohamed, A.; A Subki, A.S.R.; Mahmood, M.R. Evaluating Different TiO2 Nanoflower-Based Composites for Humidity Detection. *Sensors* **2022**, *22*, 5794, doi:10.3390/s22155794.
81. Wang, Q.; Pan, Y.Z.; Huang, S.S.; Ren, S.T.; Li, P.; Li, J.J. Resistive and Capacitive Response of Nitrogen-Doped TiO_2 Nanotubes Film Humidity Sensor. *Nanotechnology* **2011**, *22*, 025501, doi:10.1088/0957-4484/22/2/025501.
82. Bi, H.; Yin, K.; Xie, X.; Ji, J.; Wan, S.; Sun, L.; Terrones, M.; Dresselhaus, M.S. Ultrahigh Humidity Sensitivity of Graphene Oxide. *Sci Rep* **2013**, *3*, 2714, doi:10.1038/srep02714.
83. Lin, W.-D.; Liao, C.-T.; Chang, T.-C.; Chen, S.-H.; Wu, R.-J. Humidity Sensing Properties of Novel Graphene/TiO2 Composites by Sol–Gel Process. *Sensors and Actuators B: Chemical* **2015**, *209*, 555–561, doi:10.1016/j.snb.2014.12.013.
84. Lin, Y.-J.; Yang, S.-H. Carrier Transport and Photoresponse for Heterojunction Diodes Based on the Reduced Graphene Oxide-Based TiO2 Composite and p-Type Si. *Appl. Phys. A* **2014**, *116*, 91–95, doi:10.1007/s00339-013-8166-5.
85. Ghadiry, M.; Gholami, M.; Choon Kong, L.; Wu Yi, C.; Ahmad, H.; Alias, Y. Nano-Anatase TiO2 for High Performance Optical Humidity Sensing on Chip. *Sensors* **2015**, *16*, 39, doi:10.3390/s16010039.

86. Samet, M.; Kallel, A.; Serghei, A. Maxwell-Wagner-Sillars Interfacial Polarization in Dielectric Spectra of Composite Materials: Scaling Laws and Applications. *Journal of Composite Materials* **2022**, *56*, 3197–3217, doi:10.1177/00219983221090629.
87. Farahani, H.; Wagiran, R.; Hamidon, M. Humidity Sensors Principle, Mechanism, and Fabrication Technologies: A Comprehensive Review. *Sensors* **2014**, *14*, 7881–7939, doi:10.3390/s140507881.
88. Smetaniuk, D.P.; Taschuk, M.T.; Brett, M.J. Photocatalytic Titanium Dioxide Nanostructures for Self-Regenerating Relative Humidity Sensors. *IEEE Sensors J.* **2011**, *11*, 1713–1719, doi:10.1109/JSEN.2010.2095416.
89. Taschuk, M.T.; Steele, J.J.; Van Popta, A.C.; Brett, M.J. Photocatalytic Regeneration of Interdigitated Capacitor Relative Humidity Sensors Fabricated by Glancing Angle Deposition. *Sensors and Actuators B: Chemical* **2008**, *134*, 666–671, doi:10.1016/j.snb.2008.06.009.
90. Steele, J.J.; Taschuk, M.T.; Brett, M.J. Response Time of Nanostructured Relative Humidity Sensors. *Sensors and Actuators B: Chemical* **2009**, *140*, 610–615, doi:10.1016/j.snb.2009.05.016.
91. Borini, S.; White, R.; Wei, D.; Astley, M.; Haque, S.; Spigone, E.; Harris, N.; Kivioja, J.; Ryhänen, T. Ultrafast Graphene Oxide Humidity Sensors. *ACS Nano* **2013**, *7*, 11166–11173, doi:10.1021/nn404889b.
92. Olson, E.J.; Ma, R.; Sun, T.; Ebrish, M.A.; Haratipour, N.; Min, K.; Aluru, N.R.; Koester, S.J. Capacitive Sensing of Intercalated H_2O Molecules Using Graphene. *ACS Appl. Mater. Interfaces* **2015**, *7*, 25804–25812, doi:10.1021/acsami.5b07731.
93. Luryi, S. Quantum Capacitance Devices. *Applied Physics Letters* **1988**, *52*, 501–503, doi:10.1063/1.99649.
94. Fang, T.; Konar, A.; Xing, H.; Jena, D. Carrier Statistics and Quantum Capacitance of Graphene Sheets and Ribbons. *Applied Physics Letters* **2007**, *91*, 092109, doi:10.1063/1.2776887.
95. Xia, J.; Chen, F.; Li, J.; Tao, N. Measurement of the Quantum Capacitance of Graphene. *Nature Nanotech* **2009**, *4*, 505–509, doi:10.1038/nnano.2009.177.
96. Leenaerts, O.; Partoens, B.; Peeters, F.M. Adsorption of H2O, NH3, CO, NO2, and NO on Graphene: A First-Principles Study. **2007**, doi:10.48550/ARXIV.0710.1757.
97. Schedin, F.; Geim, A.K.; Morozov, S.V.; Hill, E.W.; Blake, P.; Katsnelson, M.I.; Novoselov, K.S. Detection of Individual Gas Molecules Adsorbed on Graphene. *Nature Mater* **2007**, *6*, 652–655, doi:10.1038/nmat1967.
98. Biesheuvel, P.M.; Bazant, M.Z. Nonlinear Dynamics of Capacitive Charging and Desalination by Porous Electrodes. *Phys. Rev. E* **2010**, *81*, 031502, doi:10.1103/PhysRevE.81.031502.
99. Largeot, C.; Portet, C.; Chmiola, J.; Taberna, P.-L.; Gogotsi, Y.; Simon, P. Relation between the Ion Size and Pore Size for an Electric Double-Layer Capacitor. *J. Am. Chem. Soc.* **2008**, *130*, 2730–2731, doi:10.1021/ja7106178.
100. Shao, Y.; El-Kady, M.F.; Sun, J.; Li, Y.; Zhang, Q.; Zhu, M.; Wang, H.; Dunn, B.; Kaner, R.B. Design and Mechanisms of Asymmetric Supercapacitors. *Chem. Rev.* **2018**, *118*, 9233–9280, doi:10.1021/acs.chemrev.8b00252.
101. Tian, X.; Zhu, Q.; Xu, B. "Water-in-Salt" Electrolytes for Supercapacitors: A Review. *ChemSusChem* **2021**, *14*, 2501–2515, doi:10.1002/cssc.202100230.
102. Pang, M.; Jiang, S.; Zhao, J.; Zhang, S.; Wang, R.; Li, N.; Liu, R.; Pan, Q.; Qu, W.; Xing, B. "Water-in-Salt" Electrolyte Enhanced High Voltage Aqueous Supercapacitor with Carbon Electrodes Derived from Biomass Waste-Ground Grain Hulls. *RSC Adv.* **2020**, *10*, 35545–35556, doi:10.1039/D0RA07448A.
103. Jing, L.; Zhuo, K.; Sun, L.; Zhang, N.; Su, X.; Chen, Y.; Hu, X.; Feng, R.; Wang, J. The Mass-Balancing between Positive and Negative Electrodes for Optimizing Energy Density of Supercapacitors. *J. Am. Chem. Soc.* **2024**, *146*, 14369–14385, doi:10.1021/jacs.4c00486.
104. Stoller, M.D.; Ruoff, R.S. Best Practice Methods for Determining an Electrode Material's Performance for Ultracapacitors. *Energy Environ. Sci.* **2010**, *3*, 1294, doi:10.1039/c0ee00074d.
105. Pech, D.; Brunet, M.; Durou, H.; Huang, P.; Mochalin, V.; Gogotsi, Y.; Taberna, P.-L.; Simon, P. Ultrahigh-Power Micrometre-Sized Supercapacitors Based on Onion-like Carbon. *Nature Nanotech* **2010**, *5*, 651–654, doi:10.1038/nnano.2010.162.
106. Chmiola, J.; Largeot, C.; Taberna, P.-L.; Simon, P.; Gogotsi, Y. Monolithic Carbide-Derived Carbon Films for Micro-Supercapacitors. *Science* **2010**, *328*, 480–483, doi:10.1126/science.1184126.

 doi:10.20944/preprints202511.0205.v1

107. Yoo, J.J.; Balakrishnan, K.; Huang, J.; Meunier, V.; Sumpter, B.G.; Srivastava, A.; Conway, M.; Mohana Reddy, A.L.; Yu, J.; Vajtai, R.; et al. Ultrathin Planar Graphene Supercapacitors. *Nano Lett.* **2011**, *11*, 1423–1427, doi:10.1021/nl200225j.
108. El-Kady, M.F.; Kaner, R.B. Scalable Fabrication of High-Power Graphene Micro-Supercapacitors for Flexible and on-Chip Energy Storage. *Nat Commun* **2013**, *4*, 1475, doi:10.1038/ncomms2446.
109. El-Kady, M.F.; Strong, V.; Dubin, S.; Kaner, R.B. Laser Scribing of High-Performance and Flexible Graphene-Based Electrochemical Capacitors. *Science* **2012**, *335*, 1326–1330, doi:10.1126/science.1216744.
110. Wu, Z.-S.; Feng, X.; Cheng, H.-M. Recent Advances in Graphene-Based Planar Micro-Supercapacitors for on-Chip Energy Storage. *National Science Review* **2014**, *1*, 277–292, doi:10.1093/nsr/nwt003.
111. Li, H.; Liang, J. Recent Development of Printed Micro-Supercapacitors: Printable Materials, Printing Technologies, and Perspectives. *Advanced Materials* **2020**, *32*, 1805864, doi:10.1002/adma.201805864.
112. Wang, K.; Zou, W.; Quan, B.; Yu, A.; Wu, H.; Jiang, P.; Wei, Z. An All-Solid-State Flexible Micro-supercapacitor on a Chip. *Advanced Energy Materials* **2011**, *1*, 1068–1072, doi:10.1002/aenm.201100488.
113. Hong, S.Y.; Yoon, J.; Jin, S.W.; Lim, Y.; Lee, S.-J.; Zi, G.; Ha, J.S. High-Density, Stretchable, All-Solid-State Microsupercapacitor Arrays. *ACS Nano* **2014**, *8*, 8844–8855, doi:10.1021/nn503799j.
114. Kim, D.; Shin, G.; Kang, Y.J.; Kim, W.; Ha, J.S. Fabrication of a Stretchable Solid-State Micro-Supercapacitor Array. *ACS Nano* **2013**, *7*, 7975–7982, doi:10.1021/nn403068d.
115. Park, S.; Lee, H.; Kim, Y.-J.; Lee, P.S. Fully Laser-Patterned Stretchable Microsupercapacitors Integrated with Soft Electronic Circuit Components. *NPG Asia Mater* **2018**, *10*, 959–969, doi:10.1038/s41427-018-0080-z.
116. Xiao, X.; Li, T.; Yang, P.; Gao, Y.; Jin, H.; Ni, W.; Zhan, W.; Zhang, X.; Cao, Y.; Zhong, J.; et al. Fiber-Based All-Solid-State Flexible Supercapacitors for Self-Powered Systems. *ACS Nano* **2012**, *6*, 9200–9206, doi:10.1021/nn303530k.
117. Teymoory, P.; Zhao, J.; Shen, C. How Practical Are Fiber Supercapacitors for Wearable Energy Storage Applications? *Micromachines* **2023**, *14*, 1249, doi:10.3390/mi14061249.
118. Wang, L.; Tang, Y.; Li, Y.; Liu, C.; Wei, N.; Zeng, W.; Liang, D. Multifunctional Integrated Interdigital Microsupercapacitors and Self-Powered Iontronic Tactile Pressure Sensor for Wearable Electronics. *ACS Appl. Mater. Interfaces* **2022**, *14*, 47136–47147, doi:10.1021/acsami.2c15117.
119. Tadesse, M.G.; Lübben, J.F. Review on Hydrogel-Based Flexible Supercapacitors for Wearable Applications. *Gels* **2023**, *9*, 106, doi:10.3390/gels9020106.
120. Chaney, L.E.; Hyun, W.J.; Khalaj, M.; Hui, J.; Hersam, M.C. Fully Printed, High-Temperature Micro-Supercapacitor Arrays Enabled by a Hexagonal Boron Nitride Ionogel Electrolyte. *Advanced Materials* **2024**, *36*, 2305161, doi:10.1002/adma.202305161.
121. Flores-Diaz, N.; De Rossi, F.; Das, A.; Deepa, M.; Brunetti, F.; Freitag, M. Progress of Photocapacitors. *Chem. Rev.* **2023**, *123*, 9327–9355, doi:10.1021/acs.chemrev.2c00773.
122. Zhang, X.; Song, W.; Tu, J.; Wang, J.; Wang, M.; Jiao, S. A Review of Integrated Systems Based on Perovskite Solar Cells and Energy Storage Units: Fundamental, Progresses, Challenges, and Perspectives. *Advanced Science* **2021**, *8*, 2100552, doi:10.1002/advs.202100552.
123. Boruah, B.D.; Mathieson, A.; Wen, B.; Jo, C.; Deschler, F.; De Volder, M. Photo-Rechargeable Zinc-Ion Capacitor Using 2D Graphitic Carbon Nitride. *Nano Lett.* **2020**, *20*, 5967–5974, doi:10.1021/acs.nanolett.0c01958.
124. Prakash, H.C.; Kumar, M.S.; Lin, T.-W.; Batabyal, S.K. Photo-Assisted Capacitive Performance of V2O5 Supercapacitor. *Electrochimica Acta* **2023**, *469*, 143229, doi:10.1016/j.electacta.2023.143229.
125. Rani, J.R.; Das, N.C.; Kim, M.; Thangavel, R.; Kim, S.T.; Lee, Y.S.; Jang, J.-H. Realizing High Energy Density Supercapacitors Assisted by Light-Induced Charging. *Journal of Power Sources* **2023**, *576*, 233197, doi:10.1016/j.jpowsour.2023.233197.
126. Yuan, Y.; Jiang, L.; Li, X.; Zuo, P.; Xu, C.; Tian, M.; Zhang, X.; Wang, S.; Lu, B.; Shao, C.; et al. Laser Photonic-Reduction Stamping for Graphene-Based Micro-Supercapacitors Ultrafast Fabrication. *Nat Commun* **2020**, *11*, 6185, doi:10.1038/s41467-020-19985-2.

 doi:10.20944/preprints202511.0205.v1

127. Shin, C.; Yao, L.; Lin, H.; Liu, P.; Ng, T.N. Photothermal Supercapacitors with Gel Polymer Electrolytes for Wide Temperature Range Operation. *ACS Energy Lett.* **2023**, *8*, 1911–1918, doi:10.1021/acsenergylett.3c00207.
128. Zhu, S.; Chen, M.; Wang, S.; Wu, W.; Yue, Y.; Fu, Q.; Jiang, S.; He, S.; Wu, Q.; Xiao, H.; et al. Boosting Photothermal Conversion and Energy Storage in MXene Electrodes through Softened Wood toward Solar-Enhanced Flexible Supercapacitor. *Industrial Crops and Products* **2024**, *221*, 119289, doi:10.1016/j.indcrop.2024.119289.
129. Beidaghi, M.; Gogotsi, Y. Capacitive Energy Storage in Micro-Scale Devices: Recent Advances in Design and Fabrication of Micro-Supercapacitors. *Energy Environ. Sci.* **2014**, *7*, 867, doi:10.1039/c3ee43526a.